International Journal of Nanomedicine

Dovepress
open access to scientific and medical research

Open Access Full Text Article

ORIGINAL RESEARCH

# Bifunctional Therapeutic Application of Low-Frequency Ultrasound Associated with Zinc Phthalocyanine-Loaded Micelles

This article was published in the following Dove Press journal:
*International Journal of Nanomedicine*

International Journal of Nanomedicine downloaded from https://www.dovepress.com/
For personal use only.

Yugo A Martins[1]
Maria JV Fonseca[1]
Theo Z Pavan[2]
Renata FV Lopez[1]

[1]School of Pharmaceutical Sciences of Ribeirao Preto, University of Sao Paulo, Ribeirao Preto, São Paulo, 14040-903, Brazil; [2]School of Philosophy, Sciences and Letters of Ribeirao Preto, University of Sao Paulo, Ribeirao Preto, Sao Paulo, 14090-900, Brazil

**Purpose:** Sonodynamic therapy (SDT) is a new therapeutic modality for the noninvasive cancer treatment based on the association of ultrasound and sonosensitizer drugs. Topical SDT requires the development of delivery systems to properly transport the sonosensitizer, such as zinc phthalocyanine (ZnPc), to the skin. In addition, the delivery system itself can participate in sonodynamic events and influence the therapeutic response. This study aimed to develop ZnPc-loaded micelle to evaluate its potential as a topical delivery system and as a cavitational agent for low-frequency ultrasound (LFU) application with the dual purpose of promoting ZnPc skin penetration and generating reactive oxygen species (ROS) for SDT.

**Methods:** ZnPc-loaded micelles were developed by the thin-film hydration method and optimized using the Quality by Design approach. Micelles' influence on LFU-induced cavitation activity was measured by potassium iodide dosimeter and aluminum foil pits experiments. In vitro skin penetration of ZnPc was assessed after pretreatment of the skin with LFU and simultaneous LFU treatment using ZnPc-loaded micelles as coupling media followed by 6 h of passive permeation of ZnPc-loaded micelles. The singlet oxygen generation by LFU irradiation of the micelles was evaluated using two different hydrophilic probes. The lipid peroxidation of the skin was estimated using the malondialdehyde assay after skin treatment with simultaneous LFU using ZnPc-loaded micelles. The viability of the B16F10 melanoma cell line was evaluated using resazurin after treatment with different concentrations of ZnPc-loaded micelles irradiated or not with LFU.

**Results:** The micelles increased the solubility of ZnPc and augmented the LFU-induced cavitation activity in two times compared to water. After 6 h ZnPc-loaded micelles skin permeation, simultaneous LFU treatment increased the amount of ZnPc in the dermis by more than 40 times, when compared to non-LFU-mediated treatment, and by almost 5 times, when compared to LFU pretreatment protocol. The LFU irradiation of micelles induced the generation of singlet oxygen, and the lipoperoxidation of the skin treated with the simultaneous LFU was enhanced in three times in comparison to the non-LFU-treated skin. A significant reduction in cell viability following treatment with ZnPc-loaded micelles and LFU was observed compared to blank micelles and non-LFU-treated control groups.

**Conclusion:** LFU-irradiated mice can be a potential approach to skin cancer treatment by combining the functions of increasing drug penetration and ROS generation required for SDT.

**Keywords:** sonodynamic therapy, nanocarrier, topical delivery, reactive oxygen species, skin cancer

Correspondence: Renata FV Lopez
University of São Paulo, School of Pharmaceutical Sciences of Ribeirao Preto, Av. Do Café s/n, Ribeirao Preto, SP 14040-903, Brazil
Tel +55(16)3315-4202
Email rvianna@fcfrp.usp.br

## Introduction

Low-frequency ultrasound (LFU), that is, ultrasound in the 20–100 kHz range, has been extensively studied as a physical method to overcome the stratum corneum,[1,2]



© 2020 Martins et al. This work is published and licensed by Dove Medical Press Limited. The full terms of this license are available at https://www.dovepress.com/terms.php and incorporate the Creative Commons Attribution – Non Commercial (unported, v3.0) License (http://creativecommons.org/licenses/by-nc/3.0/). By accessing the work you hereby accept the Terms. Non-commercial uses of the work are permitted without any further permission from Dove Medical Press Limited, provided the work is properly attributed. For permission for commercial use of this work, please see paragraphs 4.2 and 5 of our Terms (https://www.dovepress.com/terms.php).

the outermost layer of the skin, which provides an effective barrier to the penetration of drugs. This method is known as sonophoresis or low-frequency sonophoresis.[1]

The application of LFU in a coupling medium over the skin creates cavitation microbubbles that collapse asymmetrically against the skin surface, resulting in powerful microjets that disorganize the stratum corneum and modify skin permeability.[1,3,4] Several studies have proposed that LFU creates a network of hydrophilic porous in the skin, known as localized transport regions (LTRs), through which drug molecules can diffuse and reach systemic circulation.[5]

LFU application to the skin can be performed in two modes: (i) simultaneous treatment, which corresponds to a simultaneous application of ultrasound through a coupling medium containing the drug; and (ii) pretreatment, which ultrasound is used to permeabilize skin before drug administration.[1,2] The simultaneous treatment enhances drug transport by structural alterations of the skin and convection-related mechanisms whereas pretreatment, which drug is administered after skin permeabilization, relies only on skin structural changes induced by ultrasound.[1,6]

Besides the application to skin drug delivery, LFU can serve as a source of energy for the sonodynamic therapy (SDT) of skin tumors.[7–9] SDT is a novel approach for cancer treatment based on ultrasonic activation of sonosensitizer drugs.[10–12] The concept of SDT is similar to the photodynamic therapy: upon the sensitizer activation by light, the generated reactive oxygen species (ROS) induces oxidative injury to bioorganic molecules, resulting in cell death.[10,13] However, compared to light, ultrasound has deeper tissue penetration, resulting in a greater potential of SDT for non-invasive therapy of both superficial[14,15] and non-superficial tumors.[16,17] Specifically, in the cases of skin tumors, SDT has shown to be more efficacious to treat deeper seated or highly pigmented tumors such as malignant melanoma than photodynamic therapy.[14,15,18]

LFU is, however, rarely used in SDT, with high-frequency ultrasound being the most studied, although less energetic. It is known that the tissue penetration depth of the LFU is greater than that of the high-frequency ultrasound.[19–21] This deeper penetration of LFU can be advantageous for the SDT of cutaneous tumors, which are installed in the deep layers of the skin.

The mechanisms by which SDT with LFU lead to the death of tumor cells are not, however, clearly known. Cell death may be associated with the generation of ROS, as with the application of high-frequency ultrasound. Inertial cavitation caused by the application of LFU in a medium can generate very reactive hydroxyl radicals. These radicals can decompose the sonosensitizer and form other free radicals from the molecules of the sonosensitizer.[22] However, there is no evidence in the literature of the generation of singlet oxygen or radicals derived from the sonosensitizer from the LFU irradiation of organic model sonosensitizers, such as porphyrins and their derivatives (for example, porphimer, hematoporphyrin, chlorophyll, and phthalocyanine derivatives). Mechanical and thermal effects caused by the LFU may also contribute to the death of tumor cells, but these effects have not been studied in depth.

The potential of LFU to increase skin permeability and generate ROS motivated us to evaluate its simultaneous applicability as a skin penetration enhancer of the sonosensitizer and as an energy source for SDT. Accordingly, zinc phthalocyanine (ZnPc), a well-known photosensitizing drug with a high quantum yield of singlet oxygen production,[23] was elected as the sonosensitizing drug model for this work.

As most sensitizing agents, ZnPc belongs to class IV of the biopharmaceutical classification system, characterized by low solubility in water and low permeability.[24] Therefore, ZnPc delivery has to be assisted by formulations that allow proper solubilization of the drug in the biological medium. To avoid the prolonged photosensitivity caused by systemic administration, ZnPc has been proposed for the topical treatment of skin diseases.[25,26] Such topical formulations would permit non-invasive treatment, simple application, easy accessibility of light or ultrasound exposure, and increased drug concentration at the site of the disease, restricting adverse effects to the site of application.[24]

In this work, to overcome ZnPc's poor water solubility and enable its topical administration assisted by LFU, we encapsulate ZnPc in nanometric polymeric micelles of 1.2-distearoyl-sn-glyreco-3-phosphoethanolamine-N-[amino(polyethylene glycol)-2000] (DSPE-PEG). DSPE-PEG micelles have shown to be a potential drug carrier,[27] increasing apparent aqueous solubility and enhancing cutaneous penetration of hydrophobic drugs.[28–30] We have hypothesized that associated with LFU, this micellar system can yet facilitate the cavitation process because of the co-polymer surface properties,[31] improving the creation of transient pathways in the skin and facilitating the penetration of the sensitizing agent. Moreover, we investigate for the first time, the potential of the LFU irradiation of ZnPc-loaded micelles in

generating reactive oxygen species and cause lipoperoxidation in the skin, events that can contribute to the death of tumor cells by SDT.

Therefore, DSPE-PEG micelles were designed to increase water solubility and cutaneous penetration of ZnPc, in addition to promoting cavitation resulting from LFU application. The dual purpose of LFU as a physical penetration enhancer and energy source for SDT was evaluated.

# Materials and Methods

## Chemicals

ZnPc, pyrene, sorbitan oleate 80 (Span 80), *N,N*-dimethyl-4-nitrosoaniline (NMA), Fluoromount, 2-thiobarbituric acid (TBA), trichloroacetic acid, 2-[4-(2-hydroxyethyl) piperazin-1-yl]ethanesulfonic acid (HEPES) and 7-hydroxy-3H-phenoxazin-3-one-10-oxide sodium salt (resazurin) were purchased from Sigma-Aldrich (St Louis, MO, USA); chloroform from Merck (Germany); DSPE-PEG 2000 from Lipoid (Ludwigshafen, Germany); polysorbate 80 (Tween 80), dimethyl sulfoxide (DMSO) and salts used to prepare the phosphate buffer solution (PBS) (sodium chloride, potassium phosphate monobasic and sodium phosphate dibasic) from Synth (São Paulo, SP, Brazil); hydroxyethylcellulose (HEC) and sodium lauryl sulfate (SLS) from Galena (Campinas, SP, Brazil); Tissue Tek (O.C.T. Compound) from Sakura (Torrance, CA, USA); potassium iodide (KI) from Vetec Química Fina (Rio de Janeiro, RJ, Brazil); aluminum foil from Thermoprat (Janiru, São Paulo, Brazil); imidazole from Acros Organics/Fischer Scientific (Morris Plains, NJ, USA); Singlet Oxygen Sensor Green (SOSG) from Thermo Fischer Scientific (Eugene, OR, USA); murine melanoma cells (B16F10) from American Type Culture Collection (Rockville, MD, USA); Penicillin, streptomycin, fetal bovine serum (FBS), trypsin 0.25% and Dulbecco's Modified Eagle Medium (DMEM) from Gibco (Grand Island, NY, USA). Purified water (18.2 $M\Omega^{-1}cm^{-1}$, Milli-Q, Direct-Q 3 UV, Millipore, Billerica, MA, USA) was used to prepare all of the solutions.

## Quantification of ZnPc

A spectrofluorimetric method for ZnPc quantification was co-validated in the range from 1 to 100 $ng.mL^{-1}$ in DMSO based on an analytical method reported in the literature.[25] Briefly, ZnPc was quantified using a spectrofluorometer (PerkinElmer LS55, Llantrisant UK), setting wavelength at 610 nm and monitoring the fluorescence emission from 630 to 800 nm. Slits were adjusted to 5 for both excitation and emission settings. The method presented linearity in the studied concentration range (y = 61.9x + 49.1, r = 0.9999), with precision and accuracy greater than 97%, quantification limit of 0.4 $ng.mL^{-1}$ and detection limit 0.13 $ng.mL^{-1}$.

For the quantification of ZnPc in the micelles, the samples were adequately diluted in DMSO. Blank micelles, without ZnPc, were evaluated in the same way and showed not to interfere in the quantification of the drug.

To quantify ZnPc in skin penetration studies, the drug was extracted from samples of viable epidermis and dermis with 2 mL of DMSO in a vortex for 2 min (IKA Works, Wilmington, NC, USA), followed by fragmentation in tissue homogenizer (IKA Works, T10 basic, Wilmington, NC, USA) for 1 min at 13,500 rpm and ultrasound bath (Quimis, Q335 model, 40 kHz, São Paulo, Brazil) for 30 min. After centrifugation at 20,000x g at 25°C for 10 min, the resulting supernatant was collected, filtered through a 0.45 µm polytetrafluoroethylene (PTFE) membrane filter and analyzed by spectrofluorimetry. To verify the percentage of ZnPc recovery from these samples, fragments of viable epidermis and dermis were contaminated with known concentrations of drug and subjected to the extraction process. The percentage of recovery from samples treated with 2.5 to 10 $ng.mL^{-1}$ of ZnPc was similar for all concentrations and skin fragments studied (ANOVA, $p > 0.05$), being 56.6 ± 7.6%, and used to calculate the correction factor of 1.77. This factor was considered for estimate ZnPc ($ng/cm^2$) in skin samples according to equation (1).

$$ZnPc = \left[\frac{(ZnPc\ concentration\ x\ Extraction\ volume)}{Permeation\ area}\right] x\ 1.77 \quad (1)$$

## Micelles Development

### Determination of DSPE-PEG Critical Micelle Concentration (CMC)

Pyrene fluorescence method was used for CMC determination of DSPE-PEG.[32] A stock solution of pyrene prepared in chloroform at the concentration of 2.5 $mg.mL^{-1}$ was prepared and 20 µL were transferred to 11 test tubes. Chloroform was evaporated under compressed air, protected from light, to give 50 µg of dry pyrene in the test tubes. A series of DSPE-PEG solutions (1–50 $\mu mol.L^{-1}$) in

HEPES buffer solution (20 mmol.L$^{-1}$, pH 7.4) were added to dry pyrene. Pyrene's final concentration in each tube was 62 µmol.L$^{-1}$. The mixtures were shaken in dark for 24 h at room temperature and then filtered through a 0.45 µm membrane to separate insoluble pyrene crystals. The fluorescence intensity of solubilized pyrene in the micellar phase was determined by spectrofluorimetry with excitation and emission wavelengths set at 339 and 390 nm, respectively. The fluorescence intensity of pyrene ($I_{390}$) was plotted against the logarithm of the DSPE-PEG concentrations (mol.L$^{-1}$) to determine DSPE-PEG CMC at the point of an abrupt increase in the fluorescence intensity of the solution.

### Preparation of ZnPc-Loaded DSPE-PEG Micelles

A mixture of different DSPE-PEG and ZnPc weights according to Table 1 was dissolved in chloroform (3 mL) in a round bottom flask (25 mL). The solvent was subsequently evaporated at 50 °C under reduced pressure (100 mbar) using a rotary vacuum evaporator (IKA Works, RV 10, Wilmington, NC, USA) at 100 rpm to obtain a thin dry film of DSPE-PEG/ZnPc on the flask wall. The resulted film was then hydrated using 3 mL of different percentage of Tween 80/Span 80 (1:3 mol) dispersions in buffer solution (HEPES, pH 7.4) in an ultrasonic bath for 30 min. ZnPc not incorporated was removed by filtration through a 0.22 µm membrane filter after 24-hour resting.

**Table 1** Box-Behnken Experimental Design for Optimization of Micelle Formulation of ZnPc

| Formulation | Coded Factors | | |
|---|---|---|---|
| | X1 | X2 | X3 |
| 1 | −1 | −1 | 0 |
| 2 | +1 | −1 | 0 |
| 3 | −1 | +1 | 0 |
| 4 | +1 | +1 | 0 |
| 5 | −1 | 0 | −1 |
| 6 | +1 | 0 | −1 |
| 7 | −1 | 0 | +1 |
| 8 | +1 | 0 | +1 |
| 9 | 0 | −1 | −1 |
| 10 | 0 | +1 | −1 |
| 11 | 0 | −1 | +1 |
| 12 | 0 | +1 | +1 |
| 13 | 0 | 0 | 0 |
| 14 | 0 | 0 | 0 |
| 15 | 0 | 0 | 0 |

| Coded factors | Uncoded factors | Levels | | |
|---|---|---|---|---|
| | | −1 | 0 | +1 |
| | | (low) | (medium) | (high) |
| $X_1$ | DSPE-PEG (mg)* | 10 | 15 | 20 |
| $X_2$ | ZnF (µg)* | 70 | 140 | 210 |
| $X_3$ | Tween 80: Span 80 (1:3 mol/mol) (%) | 0 | 0.5 | 1 |

**Note:** *Dissolved in 3 mL of chloroform.

### Micelles Experimental Design

Quality by Design driven approach was utilized for the development of micellar formulation. A three-factor, three-level factorial Box-Behnken design was employed. The mass of DSPE-PEG ($X_1$), the mass of ZnPc ($X_2$), and the percentage of Tween 80/Span 80 (1:3 mol) ($X_3$) were selected as independent critical material attributes and varied at three different levels, according to the Table 1. Micelle hydrodynamic size ($Y_1$), polydispersity index (PdI) ($Y_2$), zeta potential ($Y_3$), and concentration of ZnPc solubilized ($Y_4$) were evaluated as dependent variables.

Size and PdI were analyzed by dynamic light scattering (DLS) and the zeta potential by laser doppler microelectrophoresis, as described in more detail in the micelle characterization session. The ZnPc solubilized was quantified by spectrofluorimetry using the analytical method described above. A total of 15 experiments were prepared, and the obtained data were fitted into Design Expert software (Version 11, Stat-Ease Inc, MN, USA). Three-dimensional (3D) and bidimensional plots (2D) were obtained to establish the comprehension of the relationship between the independent variables and their interactions with the responses. Analysis of Variance (ANOVA) was carried out to estimate the significance of the mathematical model established from the response surface analysis.

The optimized formulation was chosen using the desirability function approach through post-analysis point prediction with Design Expert software by establishing the proximity of the desirability function of 1.[33] Numerical optimization was performed setting the particle size and the PdI as minimum, the zeta potential as negative and the concentration of ZnPc solubilized as maximum. Micelles were then prepared in replicates (n=4) using the optimal formulation predicted to validate the model.

## DSPE-PEG Micelles Characterization

Hydrodynamic size and size distribution were measured by dynamic light scattering (DLS) using a Nano ZS (Malvern Zetasizer Nano ZS90 series, Malvern, UK)

with a scattering angle of 90° at 25 °C. Samples were diluted 5 times in deionized water. Zeta potential was determined by the laser doppler micro-electrophoresis technique with the same instrument after diluting the samples 10 times in 1 mmol.$L^{-1}$ KCl solution. The number of particles present in the optimized dispersion was determined using a nanoparticle tracker (Malvern Instruments, NanoSight NS 300, Malvern, UK) and the Nanoparticle Tracking Analysis software (NTA 3.1) after 500-fold dilution in 20 mmol.$L^{-1}$ HEPES buffer solution pH 7.4. The concentration of ZnPc solubilized in the micelles was determined by spectrofluorimetry as described before after appropriate dilution in DMSO.

The micelles were also characterized by transmission electron microscope (TEM) (JEOL, JEM-100 CX2, Tokyo, Japan) with an accelerating voltage range of 100–200 kV. For TEM visualization, micelles were diluted 50 times, 10 µL was pipetted onto a carbon-coated copper grid and the excess of liquid was removed with filter paper. After complete drying at room temperature, the grid was negatively stained by placing it on a 20 µL droplet of 2% uranyl acetate in demineralized water for 5 min. Next, the excess liquid was removed using a filter paper and the grid was dried at room temperature before the measurement.

## Cavitational Activity of DSPE-PEG Micelles

### Potassium Iodide Dosimeter

The cavitational activity of the different coupling media used in the LFU experiments was estimated using potassium iodide (KI) dosimeter as a standard method.[34,35] In this method, when KI solution is sonicated, the generated reactive radicals oxidize the $I^-$ to produce $I_2$. The excess of $I^-$ reacts with $I_2$ to form triiodide ($I^-_3$). The concentration of $KI_3$ is quantified by UV spectrophotometry at 350 nm.

KI aqueous solution at 0.1 mol.$L^{-1}$ was used to prepare the following coupling media: SLS at 1% (w/v), HEC hydrogel at 1% (w/v), blank micelles (prepared as described before, containing 2.4 mmol.$L^{-1}$ of DSPE-PEG hydrated using 0.5% (w/v) Tween 80/Span 80 in KI solution), and optimized ZnPc-loaded micelles. The coupling media were aerated for 20 min and 1 mL of each preparation was exposed to LFU (Sonics & Materials, VCX 500, Newtown, CT USA) operating at 20 kHz, spatial average temporal average intensity ($I_{sata}$) of 10 ± 0.5 W/$cm^2$, 50% duty cycle (5 s on, 5 s off) for 1 min. The intensity of LFU was measured using calorimetry[36,37] at a duty cycle of 100%. The absorbance for $KI_3$ was measured at 350 nm after a 1:3 dilution of the samples in triplicate at room temperature using a Shimadzu spectrophotometer (UV 1800, Kyoto, Japan). Sample absorbance measurements were all normalized in relation to the respective controls (coupling media diluted and not submitted to the LFU).

### Aluminum Pit Foil

The cavitation activity of the SLS at 1%, blank micelles, and ZnPc-loaded micelles as coupling media was also indirectly determined by analyzing the pits they left on an aluminum foil when LFU-sonicated, based on published protocols.[36,37] Briefly, aluminum foil was tightly mounted onto the Franz-type diffusion cells with the opaque side facing the donor compartment. The receiver compartment was filled with PBS solution. After the addition of 1 mL of the different coupling media, LFU irradiation at $I_{sata}$ 10W/$cm^2$ and 50% duty cycle (5 s on and 5 s off) was performed for 10 s. Then, the aluminum foil was removed from the diffusion cells and fixed in a wax paper. Pictures were taken positioning a source of light 5.5 cm from the aluminum foils and the camera lens 5 cm from the specimens. Areas were calculated using Fiji software after obtaining binary images of the luminous regions in the aluminum foils (n= 3–5 determinations). Analysis of pits areas was carried out by measuring the light that crossed the pits.

## In vitro Skin Penetration Studies

### Preparation of the Skin and the Diffusion Cell Apparatus

Skin from freshly excised porcine ears was obtained from a local slaughterhouse (Fribordog, Bariri, SP, Brazil), carefully dissected to remove the subcutaneous fat and adhering tissues, washed under running tap water, stored at – 80 °C and used within one month.

Before the experiments, the skin was dermatomized at 700-µm of thickness and tightly fitted in a Franz-type diffusion cell (diffusion area of 0.9 $cm^2$), with the dermis and stratum corneum facing the receptor and donor compartment, respectively.

Stratum corneum integrity was determined by placing Ag/AgCl electrodes (In Vivo Metrics, Healdsburg, CA, USA) in contact with PBS solutions that bathed the donor and receptor compartments separated by the skin mounted on the diffusion cell and subjecting this circuit to an alternating current (100 mV, 10 Hz) using a 20 MHz

function/arbitrary waveform generator (Agilent, 33220A, Santa Clara, USA). The electric current capable of passing through the skin was measured using a multimeter (Minipa, ET 1450, São Paulo, SP, Brazil) and used to calculate the skin resistance based on the Ohm's law. Resistivity was obtained by multiplying the resistance by the area of skin available for permeation. Only the skin samples that showed a resistivity of 35 > kΩcm$^2$ were used in this study.[37]

The receptor compartment (16 mL) was filled with PBS isotonic buffer solution (10 mmol.L$^{-1}$, pH 7.4, 0.9% NaCl) containing 1% (w/v) SLS to guarantee sink conditions (ZnPc solubility in this medium is 12.5 ± 0.1 μg. mL$^{-1}$),[25] kept at room temperature and under magnetic stirring. The influence of the receptor solution on the integrity of the stratum corneum was verified by subjecting the system to the passage of alternating electric current and monitoring resistivity for up to 24 h.

The optimized ZnPc-loaded micelles used in the skin penetration experiments were prepared from 20 mg of DSPE-PEG and 210 μg of ZnPc dissolved in 3 mL chloroform to form the film in the wall of the round bottom flask after organic solvent evaporation, which was hydrated with 3 mL of Tween 80: Span 80 (1:3 mol) at 0.5% in HEPES pH 7.4. ZnPc-loaded micelles containing 15 ± 3 μg mL$^{-1}$ ZnPc were used in the experiments.

## Protocols to Assess Skin Penetration of ZnPc from the Micelles

The penetration of ZnPc into the skin was evaluated from 3 different series of experiments. In the first one, 1 mL of ZnPc-loaded micelles was applied to the donor compartment for 6 h and 24 h to evaluate passive ZnPc penetration. In experiments performed for 24 h, however, SLS was not added to the receptor solution to avoid altering the integrity of the skin (Supplementary material, Figure S1.1). In the second series, the skin was pretreated with 20 kHz LFU (Sonics & Materials, VCX 500, Newtown, CT USA) at $I_{sata}$ of 10 ± 0.5 W/cm$^2$, duty cycle 50% (5 s on, 5 s off), tip displacement from the skin surface of 10 mm immersing in 1 mL of 1% HEC hydrogel as the coupling medium. The skin was pretreated until it reached a resistivity of 1.0 ± 0.5 KΩ.cm$^2$.[37] To minimize thermal effects, the coupling medium was replaced after each minute of treatment.[37] After the pretreatment, 1 mL of ZnPc-loaded micelles was applied to the donor compartment for 6 h to evaluate ZnPc penetration under the influence of LFU pretreatment. Finally, the third series of experiments was performed using ZnPc-loaded micelles as the coupling medium. The parameters and application of the LFU were the same as those previously used in the pretreatment protocol. After skin attained 1.0 ± 0.5 KΩ. cm$^2$, 1 mL of ZnPc-loaded micelles was applied to the donor compartment for 6 h to evaluate ZnPc penetration under the influence of the LFU-ZnPc simultaneous protocol.

## Evaluating ZnPc in Skin Layers

After 6 or 24-hour contact of the ZnPc-loaded micelles with the skin, the skin surfaces were carefully rinsed with distilled water to remove the excess formulation and carefully wiped with tissue paper. The stratum corneum was separated from the skin using a validated tape stripping technique with 15 pieces of adhesive tape (Scotch shipping packaging tape 3M, St. Paul, MN, USA).[25] The tape strips containing the stratum corneum were all together immersed in 5 mL of DMSO, vortex-stirred for 2 min, and sonicated for 30 min in an ultrasonic bath. DMSO phase was filtered through a 0.45 μm membrane filter of PTFE, and the resulting filtrate was analyzed by spectrofluorimetry to determine the concentration of ZnPc in the stratum corneum.[25] The remaining skin was placed in a zip-locked plastic bag and immersed in hot water at 60°C for 1 min to separate, with the help of a spatula, the epidermis without stratum corneum (viable epidermis) of the dermis. Fragmented epidermis and dermis were separately vortex-mixed (IKA Works, Wilmington, NC, USA) for 2 min in 2 mL of DMSO, homogenized using a tissue homogenizer (IKA Works, T10 basic, Wilmington, NC, USA) for 1 min at 13,500 rpm and bath-sonicated (Quimis, Q335 model, 40 kHz, São Paulo, Brazil) for 30 min. The resulting dispersion was centrifuged at 20,000x g for 10 min, and the supernatant was filtered through a 0.45 μm PTFE membrane. Finally, the ZnPc was assayed by spectrofluorimetry to determine its penetration in the viable epidermis and in dermis according to Equation 1.

To compare passive and sonophoretic penetrations, the ZnPc flux through the skin was determined at the steady-state (after 24 h of passive experiment and 6 h of experiments with LFU) by dividing the amount of drug in the dermis by the time of penetration.

The contribution of convection and acoustic transmission in the penetration of ZnPc by the LFU-ZnPc simultaneous treatment was estimated by the difference between the ZnPc flux after LFU simultaneous treatment and the flux after LFU pretreatment.

### Confocal Scanning Laser Microscopy Analysis

For confocal fluorescence microscopy, in vitro 6-h passive and sonophoretic penetrations with ZnPc micelles were carried out as described before. Also, the skin was also subjected to LFU-ZnPc simultaneous treatment without 6-h subsequent exposure to the micelles containing ZnPc. After treatments, the skin surfaces were carefully rinsed with distilled water to remove any excess formulation. The skin penetration areas were excised, soaked in Tissue-Tek® (O.C.T. Compound) inside plastic molds, frozen in acetone and dry ice, and subsequently stored at – 80°C. Cryosections of 15-µm of thickness, perpendicular to the skin surface were made using a cryostat (Leica CM1860, Illinois, EUA). All slices received Fluoromount to prevent photobleaching during analysis. A Leica TCS SP8 confocal microscope (Mannheim, Germany) with a 20x immersion objective was used for confocal fluorescence microscopy. Samples were excited with a laser at 638 nm and the fluorescence was monitored at 640–800 nm. Untreated skin was used to adjust the parameters of the microscope so that the autofluorescence of the tissue did not interfere in the analyses.

## LFU-Mediated SDT with ZnPc-Loaded Micelles

### Singlet Oxygen Detection Assays

Singlet oxygen detection was measured by monitoring the bleaching of NMA, using imidazole as a selective acceptor of $^1O_2$.[38] Upon imidazole reaction with $^1O_2$ formed, the oxidized imidazole can bind to NMA, resulting in p-NMA bleaching. The $^1O_2$ generation was then detected by the decrease of p-NMA absorbance at 440 nm.

Solutions of NMA and imidazole at 500 µmol.L$^{-1}$ and 1000 µmol.L$^{-1}$ were respectively prepared in HEPES (20 mmol.L$^{-1}$, pH 7.4). The micelles containing or not the ZnPc were diluted in HEPES to a concentration of 4.5 µmol.L$^{-1}$ of ZnPc. To 5 mL of these micellar dispersions, 250 µL and 125 µL of the NMA and imidazole solutions were added, respectively. A control solution composed only of HEPES was also prepared with the reagents NMA and imidazole. Mixtures were irradiated with LFU at $I_{sata}$ of 10 ± 0.5 W/cm$^2$ and 50% duty cycle (5s on and 5 s off) for 2 min. The absorption (A) of dispersions was evaluated before and after LFU irradiation, at room temperature, using a spectrophotometer (Shimadzu, UV 2550, Kyoto, Japan) at 440 nm. The difference between A before and after irradiation was plotted on a graph to observe the production of singlet oxygen. The experiments were repeated 3 times with different micelles batches.

In parallel, the SOSG was also used to measure singlet oxygen formation. SOSG reacts with $^1O_2$ to form SOSG-endoperoxides with a strong fluorescence emission between 525–536 nm. For the experiments, 1 µL of a 5 mmol.L$^{-1}$ SOSG solution in methanol was added to 5 mL of the micellar dispersions containing or not ZnPc at 4.5 µmol.L$^{-1}$ in HEPES solution. As a control, the SOSG was added to 5 mL of HEPES solution. These mixtures were irradiated with LFU at $I_{sata}$ of 10 ± 0.5 W/cm$^2$ and 50% duty cycle (5 s on and 5 s off) for 1 min in microtubes and analyzed in a spectrofluorimeter (Shimadzu RF-1501, Kyoto, Japan) with excitation at 505 nm and emission in the range between 510–600 nm. Sample measurements were taken before and after the ultrasound exposition to determine the percentage change in fluorescence intensity relative to the pre-exposure intensity. The experiments were repeated 3 times with different micelles batches.

### Skin Lipid Peroxidation Assay

Lipid peroxidation of skin tissue was estimated using the malondialdehyde (MDA) assay, the major biomarker of oxidative stress.[39] In vitro LFU-ZnPc simultaneous penetration experiments (followed by 6 h of contact of ZnPc-loaded micelles with the skin) were carried out as described before. The excess formulation was removed with distilled water, the permeation area was cut into fragments, and approximately 1 mg of skin fragments were added in test tubes containing 0.1 mol.L$^{-1}$ PBS solution (pH 7.4). This suspension was then irradiated for 1 min with LFU at $I_{sata}$ of 10 W/cm$^2$ and 50% duty cycle. After irradiation, 100 µL of 70 mmol.L$^{-1}$ $FeSO_4 \cdot 7H_2O$ were added and this mixture was kept at rest for 30 min at 37°C. A volume of 500 µL of the supernatant was transferred to microcentrifuge tubes, to which 1 mL of 15% (v/v) trichloroacetic acid solution was added. After centrifugation at 16,000x g for 15 min at room temperature, 500 µL of the supernatant was transferred to glass vials containing 500 µL of 0.7% (v/v) TBA solution. The tubes were shaken for 1 min and heated at 95°C for 30 min. After cooling, the samples were analyzed for estimation of the adduct MDA-TBA formed at 532 nm using a spectrophotometer (Hitachi, U2001, Tokyo, Japan). As controls, the same experiment was performed with blank skin, not treated with ZnPc-loaded micelles, irradiated or not with LFU. The experiments were repeated 3 times with different batches of micelles and skin samples.

### In vitro Melanoma Cell Viability

Preliminary studies to evaluate LFU-mediated SDT in association with ZnPc-loaded micelles were carried out in the B16F10 murine melanoma cell line. B16F10 cells, maintained in DMEM medium supplemented with 10% FBS at 37° C in humidified 5% (v/v) $CO_2$ atmosphere were seeded into the 16 central wells of 96-well plates at the concentration of 2 x $10^4$ cells per well and incubated overnight. The medium was then removed and replaced with ZnPc-loaded micelles formulation at the ZnPc concentration range of 40–200 ng.mL$^{-1}$ in non-supplemented DMEM. The number of particles per well was kept constant at 1.3 x $10^{10}$ particles/mL. Subsequently, the cells were incubated for 4 h, the formulation removed, the wells washed twice with 0.9% (w/v) NaCl solution, and the incomplete medium was added. The cells were then treated with LFU at $I_{sata}$ of 10 ± 0.5 W/cm$^2$, 50% duty cycle (5s on and 5 s off) for 5 min using a distinct experimental setup: to avoid any thermal effect, the ultrasound transducer was placed in contact with 50 mL of distilled water in a compartment physically separated from the cell culture plate (Supplementary material, Section S2, Figure S2.1). This compartment was placed in contact with the bottom of the polystyrene culture plates. The transducer was inserted in there at a distance of 5 cm from the center of the plate.

After LFU treatment, the plates were incubated for a further 24 h and cell viability was determined using resazurin assay. The medium was removed, washed with saline solution, and replaced with resazurin solution in non-supplemented medium (1:10 (v/v)). The plates were again incubated for 3 h and analyzed using a microplate reader (Biotek, model Synergy HTX, VT, USA) at the wavelengths of excitation and emission of 530 and 590 nm, respectively.[40] In parallel, a similar protocol was carried out using ZnPc micelles at the same concentrations without LFU stimulus. Results were compared against control experiments in which cells were treated with culture medium or blank micelles only.

## Statistical Analysis

Shapiro–Wilk normality test showed that experimental values come from a population of Gaussian distribution. Results were statistically analyzed by ANOVA followed by Tukey post-test or two-tailed Student's *T* test with $p < 0.05$.

# Results

## DSPE-PEG Micelles Development

The CMC for DSPE-PEG (MW = 2788 g/mol) in HEPES solution (pH 7.4, 20 mmol.L$^{-1}$) was found to be 20 µmol.L$^{-1}$ (Supplementary material, Figure S3.1).

Table 2 shows the size, PdI, zeta potential and concentration of ZnPc solubilized in the micelles prepared from the combination of the independent variables DSPE-PEG mass and ZnPc mass, both dissolved in 3 mL of chloroform, and percentage of stabilizers according to the experimental design shown in Table 1.

The micelles dispersions showed size ranging from 12 to 155 nm, PdI from 0.173 to 1, zeta potential from −9 to −28 mV, and ZnPc solubilized from 3 to 15 µg.mL$^{-1}$ (Table 2).

Figure 1 shows the bidimensional and tridimensional response surface plots of size, PdI, zeta potential, and concentration of ZnPc solubilized in the micelles as a function of the mass of DSPE-PEG, the mass of ZnPc and the percentage of Tween 80/Span 80 (1:3 mol) used to prepare the micelles.

Regression analysis and modeling performed using these data (Supplementary material, Table S3.1) generated a quadratic model to predict the size of the micelles ($Y_1$), PdI ($Y_2$) and zeta potential ($Y_3$), according to Equations 2, 3 and 4, respectively, and a general linear equation to predict the amount of ZnPc incorporated in the micelles ($Y_4$), according to Equation 5.

**Table 2** Physicochemical Characteristics and ZnPc Concentration of DSPE-PEG Micelles

| Formulation | Size (nm) | PdI | Zeta Potential (mV) | ZnPc Concentration (µg/mL) |
|---|---|---|---|---|
| 1 | 152 | 0.232 | −26 | 3.7 |
| 2 | 145 | 0.204 | −25 | 7.1 |
| 3 | 137 | 0.253 | −25 | 7.1 |
| 4 | 138 | 0.233 | −24 | 12.9 |
| 5 | -* | 1 | −9 | 9.2 |
| 6 | -* | 1 | −10 | 8.3 |
| 7 | 141 | 0.285 | −28 | 7.7 |
| 8 | 116 | 0.327 | −24 | 5.9 |
| 9 | 41 | 1 | −11 | 5.1 |
| 10 | 12 | 0.616 | −11 | 15.1 |
| 11 | 116 | 0.279 | −25 | 3.0 |
| 12 | 119 | 0.274 | −27 | 9.8 |
| 13 | 152 | 0.173 | −26 | 9.4 |
| 14 | 128 | 0.235 | −24 | 6.4 |
| 15 | 155 | 0.206 | −25 | 9.7 |

**Note:** *No nanoparticles detected.

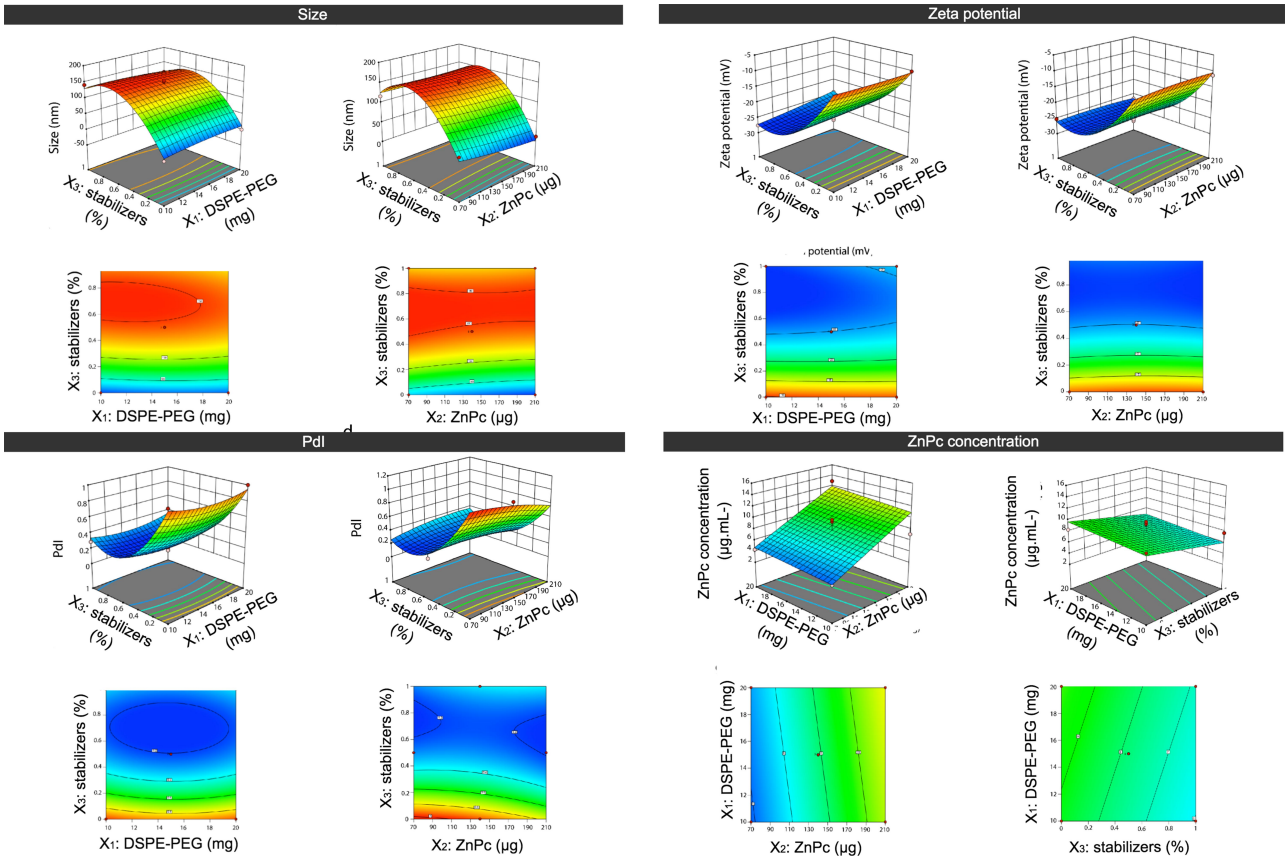



**Figure 1** 2D and 3D response surface graphs showing the effect of the independent variables studied on the size, PdI, zeta potential, and concentration of ZnPc solubilized in the micelles.

$$Y_1 = 15.69 + 419.48X_3 - 303.08X_3^2 \quad (2)$$

$$Y_2 = 1.66 - 2.57X_3 + 1.52X_3^2 \quad (3)$$

$$Y_3 = -11.21 - 47.94X_3 + 27.47X_3^2 \quad (4)$$

$$Y_4 = 0.66 + 0.05X_2 - 2.8X_3 \quad (5)$$

$X_2$ is the mass of ZnPc and $X_3$ is the percentage of stabilizers (Tween 80/Span 80) used to prepare the micelles.

From the experimental design, an optimized formulation was selected using the desirability function approach[33] (Supplementary material, Figure S3.2). The optimized formulation is shown in Table 3, as well as the responses predicted by the model and the experimental results obtained from the formulation preparation. Results showed that the experimental values were within the prediction interval calculated and demonstrate the high degree of prognostic ability of the model generated from the experimental design.

## Characterization of ZnPc-Loaded Micelles

Table 4 shows the physicochemical characteristics of the optimized ZnPc-loaded micelles compared to micelles prepared in the absence of ZnPc (blank micelles). The incorporation of ZnPc in the micelles resulted in a bluish, homogeneous, and translucent dispersion (Supplementary material, Figure S3.3). ZnPc-loaded micelles showed size, distribution profile (Supplementary material, Figure S3.4), PdI, nanoparticles concentration, and zeta potential similar to those of blank micelles (Student's $T$ test, $p > 0.05$).

Figure 2 shows a TEM image of the micelles in a dry state. It is possible to observe that most structures are spherical, of approximately 25 nm.

## Cavitational Activity of DSPE-PEG Micelles

### Potassium Iodide Dosimeter

Figure 3 shows the estimation of the cavitation measured in the different coupling media using KI dosimeter method. Cavitation activities measured in the hydrogel and the blank micelle formulations were respectively 2.5 and 2.0 times

**Table 3** Formulation Composition to Obtain the Desired Responses and Statistical Prediction Intervals for Model Confirmation

| **Formulation** | | | |
|---|---|---|---|
| **Independent Variable** | | **Optimized Level** | |
| $X_1$: DSPE-PEG (mg)* | | 20 | |
| $X_2$: ZnPc (μg)* | | 210 | |
| $X_3$: Tween 80/Span 80 (%) | | 0.5 | |
| **Response** | **Predicted values ± SD** | **Experimental values ± SD[b]** | **Prediction interval[a] (95%)** |
| Hydrodynamic size (nm) | 137 ± 15 | 138 ± 10 | 95 to 178 |
| PdI | 0.18 ± 0.09 | 0.25 ± 0.01 | 0 to 0.42 |
| Zeta potential (mV) | −25 ± 1 | −27 ± 1 | −28 to −22 |
| Mass of solubilized drug ($\mu g.mL^{-1}$) | 12 ± 2 | 13 ± 2 | 8.7 to 15.0 |

**Notes:** *Dissolved in 3 mL of chloroform; [a] Comparison by bilateral interval ($\alpha = 0.05$); [b] n = 4.

**Table 4** Physicochemical Characterization of Micelles

| **Micelles** | **Physicochemical Characteristics** | | | |
|---|---|---|---|---|
| | **Size (nm)** | **PdI** | **Particle Number/mL** | **Zeta Potential (mV)** |
| Blank | 134 ± 7 | 0.27 ± 0.01 | $3x10^{11} \pm 2x10^{11}$ | −26 ± 1 |
| ZnPc-loaded | 138 ± 10 | 0.25 ± 0.01 | $6x10^{11} \pm 2x10^{11}$ | −27 ± 1 |

Micelle composition: 2.4 $mmol.L^{-1}$ of DSPE-PEG, 0.5% (w/v) Tween 80/Span 80 (1:3) and 13 ± 2 $\mu g.mL^{-1}$ of ZnPc when it is present. Results were expressed as mean ± SD (n=3 determinations). Results were analyzed using unpaired *T* test, but no significant difference was found in the data.

higher than that in water. SLS and ZnPc-loaded micelles showed to interfere in the triiodide ions absorbance analyses; SLS itself showed an intense absorbance at 350 nm in the absence of LFU irradiation and ZnPc-loaded micelles interfere in $KI_3$ absorbance measurements after LFU irradiation. Color changes of the hydrogel and blank micelle coupling media were observed after ultrasound irradiation (Supplementary material, Section 4, Figure S4.1).

Furthermore, the evaluation of blank micelles by DLS after LFU irradiation showed a polydispersed and polymodal particles distribution, with particles ranging in size from 80 nm to 10 μm (Supplementary material, Figure S4.2). ZnPc-loaded micelles were highly polydispersed and could not be analyzed by the equipment.

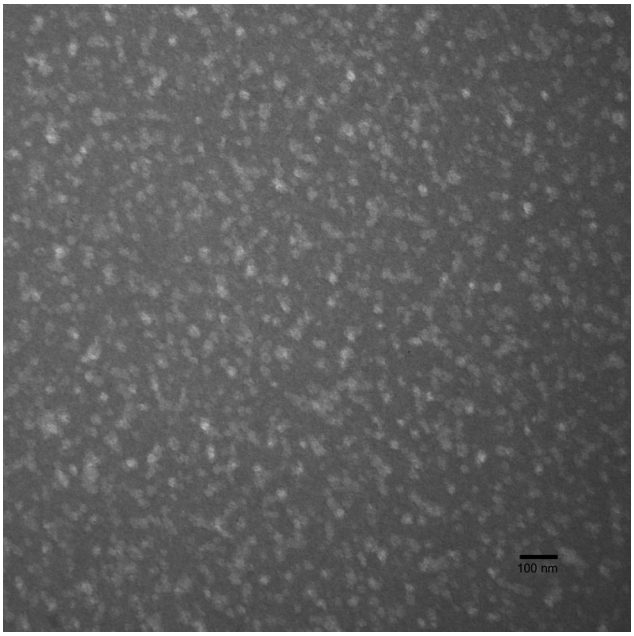



**Figure 2** TEM image of micelles at 200,000x magnification.

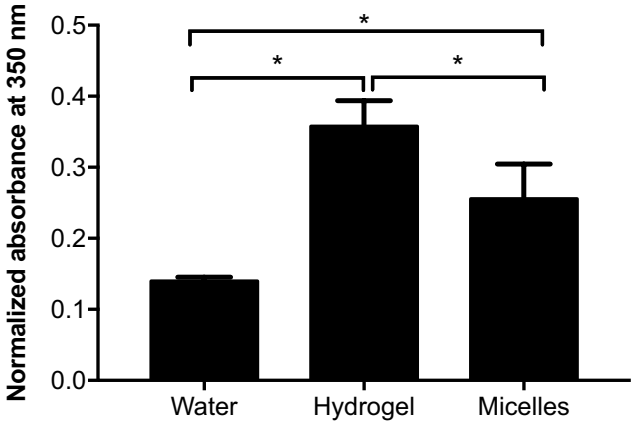



**Figure 3** Cavitation activity in coupling media used in low-frequency sonophoresis experiments. LFU parameters: 20 kHz, 10 $W/cm^2$, 50% duty cycle for 1 min. The error bars represent the standard deviation (n=3 determinations), and (*) indicate a significant difference between the $KI_3$ absorbance measured, according to ANOVA, followed by post hoc analysis using Tukey's test with $P < 0.05$ as the minimum level of significance.

## Aluminum Foil Pits

Figure 4 shows the area (in $mm^2$) of the pits formed in the aluminum foil after 10 s of LFU sonication in the presence of SLS at 1%, blank and ZnPc-loaded micelles. The pits represent physical evidence of the effects of cavitation. The pit area formed after the LFU irradiation of ZnPc-loaded micelles was 7 and 2 times larger than that formed after the irradiation of the SLS and the blank micelle, respectively. In comparison with SLS, the pit area formed after the LFU irradiation of the blank micelles was 3.3

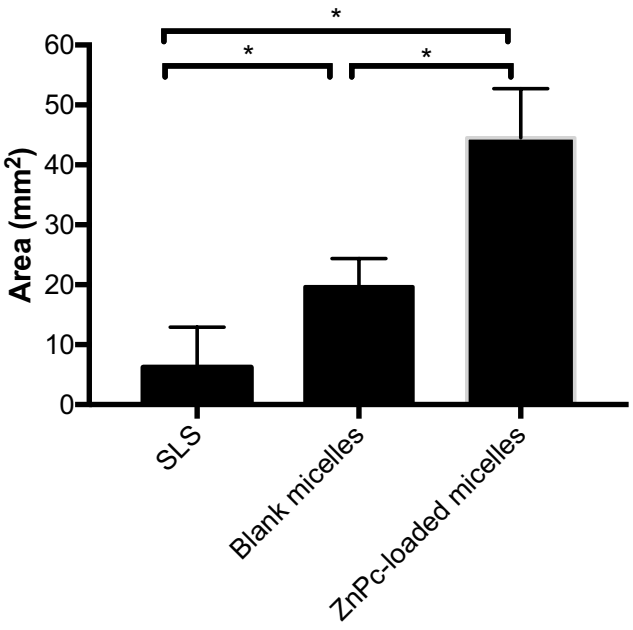



**Figure 4** Area of the aluminum foil pits after sonication of SLS solution, blank micelles, and ZnPc-loaded micelles with LFU. LFU parameters: 20 kHz, 10 W/cm$^2$, 50% duty cycle for 10 s. The error bars represent the standard deviation (n = 3–5 determinations), and (*) indicate a significant difference, according to ANOVA, followed by post hoc analysis using Tukey's test with $p < 0.05$ as the minimum level of significance.

times greater. Representative images of the pits in the aluminum foil for each coupling media analyzed can be visualized in the Supplementary material, Figure S4.3.

## In vitro Penetration Studies

Table 5 shows ZnPc recovered from the different skin layers after passive and sonophoretic treatments in both modes of LFU application: pretreatment, using hydrogel as a coupling medium, and simultaneous, using ZnPc-loaded micelles as a coupling medium.

Considering the same experimental time, treatment with LFU, regardless of the mode of application, resulted in greater penetration of ZnPc into the dermis (Table 5). The simultaneous treatment of LFU-ZnPc was what made possible the higher penetration of the drug through the epidermis, allowing 40.5 times more ZnPc to reach the dermis than passive treatment and 4.5 times more than pretreatment with LFU.

Passive treatment resulted in the accumulation of ZnPc in the epidermis (stratum corneum and viable epidermis) higher than pretreatment with LFU. However, 99% of the drug that entered was trapped in this layer and failed to reach the dermis. The treatment with the LFU led to similar amounts of ZnPc in each layer of the skin, indicating the reach of the steady-state when the skin was submitted to the LFU for 6 h.

It was not possible to quantify the ZnPc in the receptor solution after the experiments with the analytical method used. To calculate the drug flux through the skin, the amount of drug in the dermis at the steady-state was considered. Thus, Table 5 also shows the ZnPc in the different skin layers after 24 h of passive treatment (steady-state) so that the flux could be calculated.

The flux of ZnPc through the skin was about 10, 30, and 110 ng.cm$^{-2}$.h$^{-1}$ after passive treatment, LFU pretreatment, and LFU-ZnPc simultaneous treatment, respectively. It can be observed that, in comparison to passive experiment, pretreatment with LFU increased ZnPc flux through the skin by approximately 3-fold while LFU-ZnPc simultaneous treatment augmented it by 11-fold.

The contribution of the acoustic and convective flow to the ultrasonic transport of ZnPc when the simultaneous treatment was applied was 80 ng.cm$^{-2}$.h$^{-1}$, corresponding to approximately 70% of the total drug transport by this method.

Figure 5 shows the distribution of ZnPc in the skin after passive (A), LFU pretreatment (B), and LFU-ZnPc simultaneous 6-h treatments by confocal microscopy (D).

**Table 5** ZnPc Accumulated in the Different Layers of the Skin After Passive, Pretreatment with LFU, and LFU-ZnPc Simultaneous Application

| Skin Layer | ZnPc Accumulated (ng/cm$^2$) | | | |
|---|---|---|---|---|
| | Passive | | LFU (6 h) | |
| | 6 h | 24 h | Pretreatment | Simultaneous |
| Stratum corneum | 366 ± 130$^{a}$ | 471 ± 26$^{a\#}$ | 98 ± 8$^{b}$ | 744 ± 307$^{c}$ |
| Viable epidermis | 396 ± 39 | 100 ± 28$^{a}$ | 104 ± 12$^{a}$ | 344 ± 143 |
| Dermis | 8 ± 2$^{\#}$ | 136 ± 72$^{a}$ | 72 ± 34$^{a}$ | 324 ± 227$^{b}$ |

**Notes:** Results were expressed as mean ± SD from 5 to 7 experiments; *a, b* or *c* indicate significant differences in relation to data presented in the same row; therefore, equal letters in the same raw indicate that data do not show significant difference; (#) indicates a significant difference in relation to the data presented in relation to the same column. Results were analyzed using ANOVA, followed by post hoc analysis using Tukey's test with $p<0.05$ as the minimum level of significance.

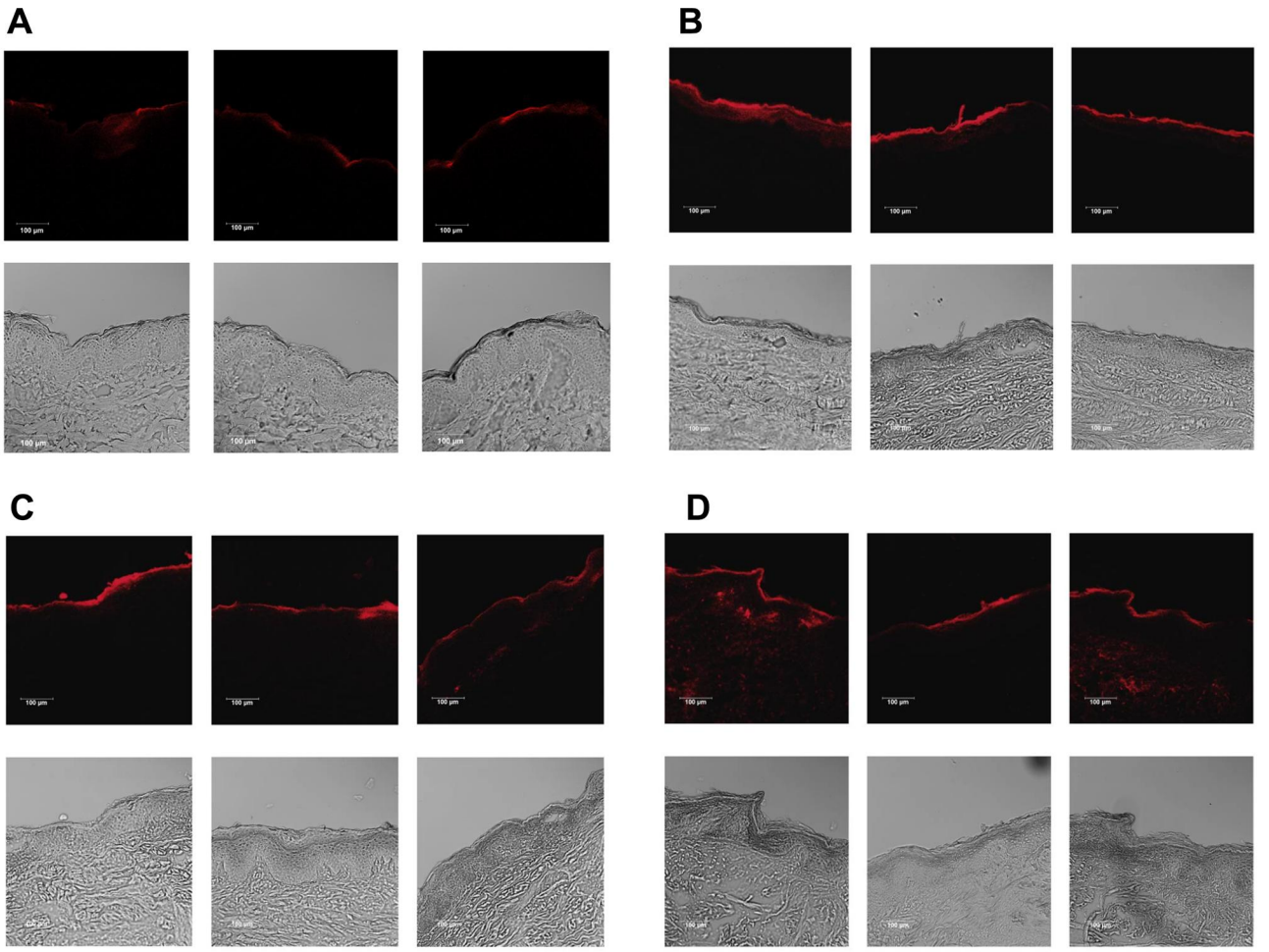



**Figure 5** Representative confocal images of 15 µm thickness cryo-sections perpendicular to the skin surface after passive and sonophoretic penetrations with ZnPc-loaded micelles. ZnPc fluorescence was observed in the red channel (λexc = 638 λem = 640–700 nm) in 20 x magnification. (**A**) 6-h passive penetration; (**B**) LFU pretreatment with hydrogel followed by 6-h penetration; (**C**) LFU-ZnPc simultaneous treatment evaluated immediately after LFU application; (**D**) LFU-ZnPc simultaneous treatment followed by 6-h penetration.

Skin treated with LFU-ZnPc simultaneous protocol and evaluated immediately after this application, without further contact with the ZnPc formulation, can also be observed in this figure (C).

The fluorescence of ZnPc, in red, can be observed over the entire length of the skin after LFU-simultaneous treatment (Figure 5C and 5D), with greater intensity in the deeper layers when it is followed by 6-h contact with the ZnPc-loaded micelles (Figure 5D). Pretreatment with LFU followed by contact with the ZnPc micellar formulation for 6 h (Figure 5B) shows a more homogeneous and intense distribution of ZnPc in the stratum corneum and viable epidermis than that presented after passive treatment (Figure 5A). This, in turn, shows a very heterogeneous distribution of ZnPc, located mainly in some furrows of the skin.

Note that the microscopy confocal images were obtained to show the distribution of ZnPc across the skin and do not reflect the actual amount of ZnPc. We cannot correlate the quantitative results from the in vitro penetration studies with the images because of the following points:

1. The histologic sections obtained do not represent the total amount of drug in the skin once only a thin fragment of the skin is analyzed while the skin layers are completely processed for drug extraction and analysis;
2. The high proclivity of polymeric micellar systems to accumulate in skin appendages, resulting in a highly heterogeneous distribution of the nanoparticles in certain sites of the skin;
3. The LTRs formed in the skin after LFU application are also heterogeneously formed in the skin.

## LFU-Mediated SDT with ZnPc-Loaded Micelles

### Singlet Oxygen Production

Figure 6 shows the singlet oxygen generation, monitored by the NMA bleaching method (Figure 6A) and by the increase of SOSG fluorescence (Figure 6B), in solution and micelles dispersions irradiated with LFU. Regardless of the method used to detect singlet oxygen in the face of LFU irradiation, a significant $^1O_2$ production was observed in both ZnPc-loaded and blank micelles groups compared to HEPES solution.

### Skin Lipid Peroxidation Assay

The effect of LFU and ZnPc on the skin's lipid peroxidation is shown in Figure 7. It can be observed that the sole LFU irradiation of the skin did not significantly increase skin lipid peroxidation when compared to the non-treated control skin. However, previous treatment of the skin by simultaneous LFU-ZnPc significantly increased lipid peroxidation of the skin by almost 3-fold.

### In vitro Melanoma Cell Viability

Figure 8 shows the viability of B16F10 murine melanoma cells after treatment with different concentrations of ZnPc-loaded micelles irradiated or not with LFU. It is possible to observe that the irradiation of LFU in cells treated with ZnPc-loaded micelles at 125 ng.mL$^{-1}$ or more significantly reduced the percentage of viable cells to approximately 60% (Figure 8B). No cytotoxic effect was observed in the cells not treated with LFU, regardless of the concentration of ZnPc used (Figure 8A). The irradiation of blank micelles (control group) did not induce any reduction in the percentage of viable cells.

## Discussion

The use of micelles prepared from amphiphilic co-polymers is an attractive approach for the solubilization of poorly soluble drugs such as ZnPc.[41–44] DSPE-PEG is an FDA approved amphiphilic co-polymer for internal use that consists of a hydrophilic PEG block and a hydrophobic phospholipid moiety made up by two long fatty acyl chains.[45] In aqueous solution, the highly hydrated chains of PEG form a dense brush-like corona/shell in the surface of micelles, conferring a protective barrier around the core of the micelle and its cargo. In topical applications, this PEG arrangement may increase the stability of the micelles in contact with the skin. Moreover, the choice for using DSPE-PEG to obtain micelles in this study was mainly made based on its hydrophilic characteristics, compatible with LTRs created by skin irradiation with LFU, and low CMC, which could permit the use of less amount of phospholipids to yield a micellar drug delivery system with only 1% (w/v) of lipid content for LFU-sonophoretic delivery.

The DSPE-PEG CMC determined in our experiments (20 μmol.L$^{-1}$) (Supplementary material, Figure S3.1) was of the same order of magnitude as others reported in the literature for DSPE-PEG of similar molecular weight.[32,41] Such low CMC value implies greater thermodynamic stability, which allows the micelles to maintain their integrity

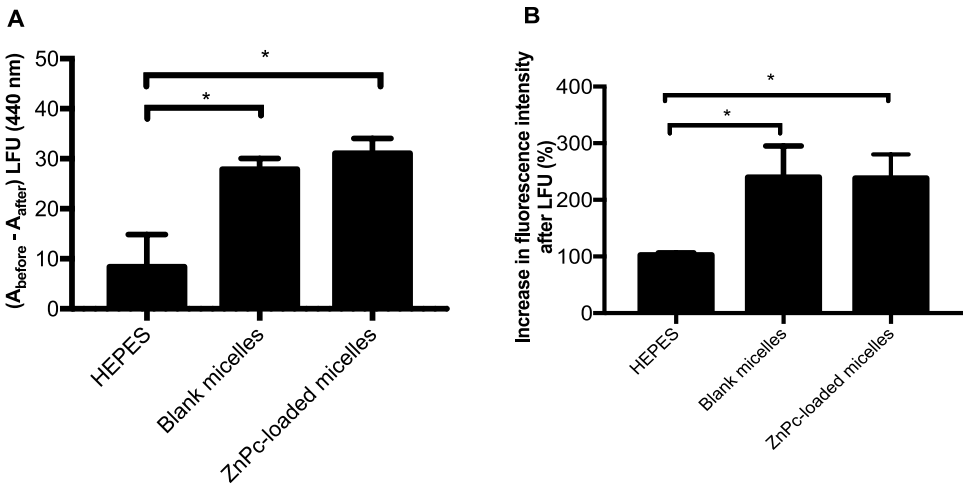



**Figure 6** Singlet oxygen detection in solution and micellar dispersions, containing or not ZnPc, after irradiation with LFU. (**A**) detection by the method of NMA bleaching after 2 min of LFU irradiation. (**B**) detection by SOSG fluorescence increase after 1 min of LFU irradiation. LFU parameters: 20 kHz, 10±0.5 W/cm$^2$, 50% duty cycle. The error bars represent the standard deviation (n = 3 determinations), and (*) indicates a significant difference according to ANOVA followed by post hoc analysis using Tukey's test with $P < 0.05$ as the minimum level of significance.

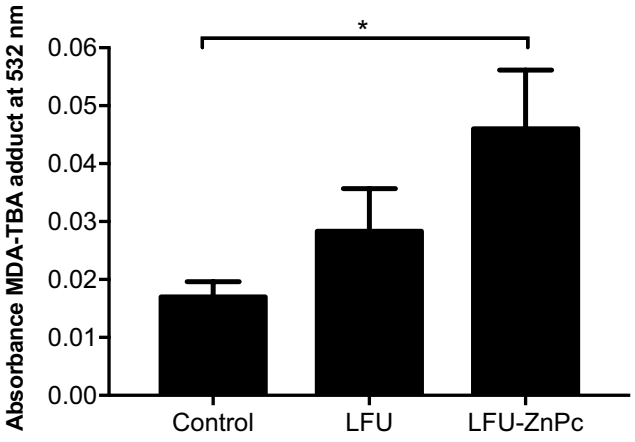



**Figure 7** Effect of LFU and ZnPc on skin lipid peroxidation. Legend: Control: non-treated skin, LFU: skin irradiated with LFU, LFU-ZnPc: skin previously treated by LFU-ZnPc simultaneous protocol. LFU parameters: 20 kHz, 10 W/cm$^2$, 50% duty cycle for 1 min. The error bars represent the standard deviation (n = 3–4 determinations), and (*) indicates significant difference according to ANOVA followed by post hoc analysis using Tukey's test with $P < 0.05$ as the minimum level of significance.

upon heavy dilutions such as in experimental procedures or systemic administration.[45] The experimental design was then built to have DSPE-PEG concentrations 55 to 110 times greater than DSPE-PEG CMC, estimating that the dispersion to be formed presents a high concentration of micelles and thus allows the solubilization of high concentrations of ZnPc. Due to its high lipophilicity, ZnPc was then dissolved in the same organic solvent as DSPE-PEG to prepare the micelles by the hydration method of the lipid film.[41,46] The ZnPc concentration range chosen for the experimental design (Table 1) was that which resulted in visually homogeneous films in the flask after evaporation of the organic solvent.

As dependent variables or responses to the process factors (mass of DSPE-PEG, mass of ZnPc, and percentage of Tween 80/Span 80), size, PdI, zeta potential, and solubilization of ZnPc were considered. These responses are important for the stability of the micelles,[33,47] interactions with the skin, and penetration of the encapsulated drug (ZnPc). The lower the polydispersity and the higher the zeta potential, the greater the stability of the micelles.[33] The smaller the size of the micelles and the higher the amount of solubilized drug, the greater the surface area in contact with the skin,[33] the concentration gradient[33] and likely the skin penetration of the ZnPc.

The figure obtained when the dependent variables are plotted as a function of one or more process factors is called response surface graph (Figure 1). It allowed us to evaluate the relationships between the mass of DSPE-

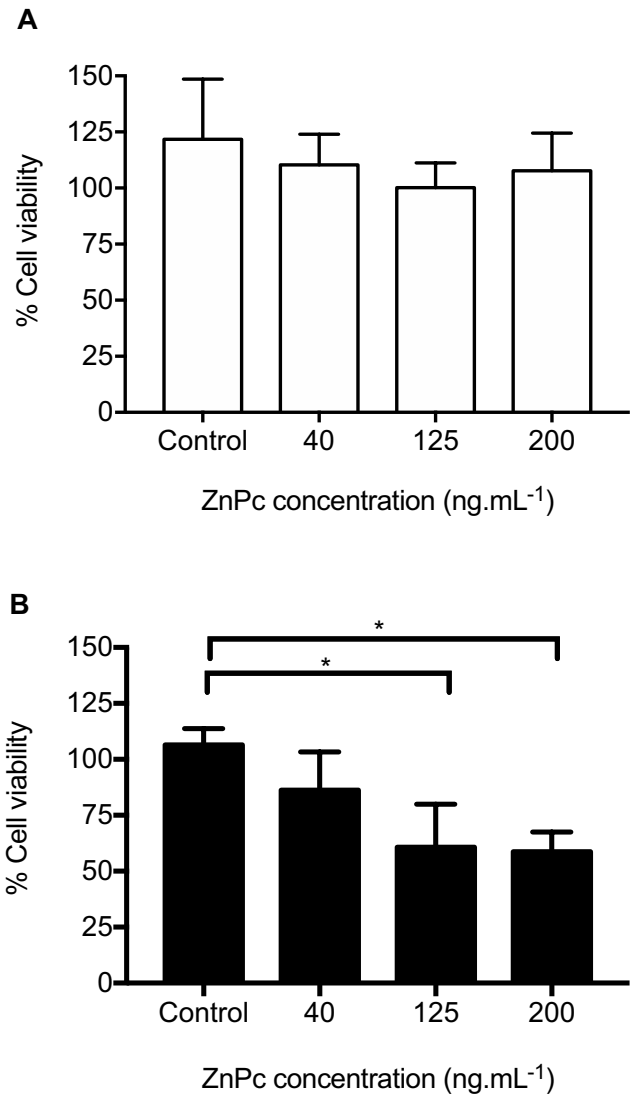



**Figure 8** Cell viability of B16F10 melanoma cell line non-irradiated (**A**) and irradiated with LFU (**B**) after treatment with different concentrations of ZnPc-loaded micelles. LFU parameters: 20 kHz, 10 W/cm$^2$, 50% duty cycle for 5 min. The error bars represent the standard deviation (n = 3 determinations), and (*) indicates a significant difference according to ANOVA using Dunnett's multiple comparisons ($\alpha = 0.05$).

PEG, the mass of ZnPc and the percentage of Tween 80/Span 80 (stabilizers), used to prepare the micelles, and the responses selected to optimize the micellar dispersion, that is, size, PdI, zeta potential and solubilized ZnPc concentration. Linear regressions and modeling (Supplementary material, Table S3.1) analysis performed with this data generated Equations 2 to 5.

It is possible to note in Equation 2 and Figure 1 that the hydrodynamic size of the micelles increased as the concentration of stabilizers increased until an intermediate percentage (0.5%). High concentrations of stabilizers, however, end up decreasing the size of the micelles. It is

probable that the addition of Tween/Span up to intermediate levels can primarily enlarge the micelle size because of their intercalation within DSPE-PEG micelle corona regions. The excess of these surfactants may, however, no longer interact with DSPE-PEG micelles and form smaller non-ionic micelles of Tween/Span or simply start to solubilize the DSPE-PEG aggregates. As a result, the percentage of surfactants also significantly influenced, following similar quadratic models, the PdI and the zeta potential of the micelles, as shown in Equations 3 and 4, respectively, and Figure 1.

For PdI, intermediate percentages of surfactants interacting with DSPE-PEG micelles led to a decrease in PdI; high percentages, on the other hand, increase polydispersion, probably due to the reasons discussed previously. Zeta potential, in turn, became more negative as the levels of stabilizers ($X_3$) increased. Again, this change can be attributed to Tween/Span and DSPE-PEG interactions, which can modify the distribution of the buffer solution ions, increasing the zeta potential in modulus. This additional electrical stability provided by Tween/Span can prevent precipitation of the DSPE-PEG micelles, which, in the absence of stabilizing agents, precipitate when stored for more than seven days at 25°C.[48]

In addition to the influence of the mixture of Tween/Span surfactants on the size, PdI and zeta potential of the micelles, this variable affected the concentration of ZnPc solubilized in the micelle ($Y_4$). The concentration of ZnPc is also influenced by the amount of drug ($X_2$) used in preparing the micelles, as described in the general linear equation (Equation 5) predicted for this response from the regression analyzes. Based on Equation 5 and Figure 1, it is possible to affirm that the increase of ZnPc ($X_2$) caused a gradual increase in the concentration of drug in the micelle. However, increasing the percentage of stabilizers ($X_3$) showed to reduce the concentration of ZnPc solubilized. This result suggests that Tween/Span may compete against the drug for the DSPE-PEG micelles. Therefore, increasing percentage of stabilizers in the formulation would result in reduced ZnPc solubility in the micelles. This result confirms the hypothesis the surfactants interact with the micelles, altering its hydrodynamic size, PdI and zeta potential in function of the surfactant concentration.

After knowing the influence of the independent variables on the dependent variables, an optimized formulation was then selected using the desirability function approach.[33] The optimized formulation was then established, as shown in Table 4. It is composed of approximately 3 $mmol.L^{-1}$ of Tween 80 (MW 1310 $g.mol^{-1}$) and Span 80 (MW 429 $g.mol^{-1}$) and 2.4 $mmol.L^{-1}$ of DSPE-PEG. Therefore, the surfactants/DSPE-PEG molar ratio calculated was 2.5:1. This high proportion of surfactants associated with the preparation method of hydration of the lipid film suggest that the surfactants solubilized part of the lipid bilayers formed by DSPE-PEG in the aqueous medium, therefore yielding the formation of micelles. Several studies have reported DSPE-PEG micelles with similar physicochemical characteristics to the micelles reported in this current work.[42–44,49]

The analysis by TEM (Figure 2) showed that the micelles appear as small spherical structures, which is in agreement with other studies.[43,50,51] The size of the micelles obtained by TEM was, however, about 5-fold smaller than that obtained by DLS. This is due to the differences between the radius of the micelles in the dry state, as in the analysis by TEM, and hydrated, as in the analysis by DLS. In TEM analysis, the hydration of the pegylated portion of the micelles is not observed; therefore, the hydrodynamic size is only determined by DLS. Moreover, the core and the hydrophilic PEG corona could not be distinguished in the TEM images due to the low contrast in the electronic density between the polymer blocks.[43]

The optimized micelles solubilized approximately 15 $\mu g.mL^{-1}$ of ZnPc (Table 3). This corresponds to 4-fold more ZnPc than the micelles of DSPE-PEG 5000 containing the drug reported in the literature.[49] However, compared to nanoemulsions, ZnPc concentration found in the micelles was up to 4-fold lower.[25,52] Although the concentration of ZnPc solubilized in such oil-containing delivery systems is higher than that found in the micelles, it is reasonable to infer that the lipid content of emulsions could restore the LTRs formed in the skin by LFU treatment, resulting in a drastic reduction of drug transport through the skin by sonophoresis. Indeed, some studies have suggested that the sonophoretic transport of drugs from liposomes resulted in lower drug penetration.[53]

Because cavitation is the main phenomena involved in the creation of LTRs in the skin during LFU application,[1] the influence of developed micelles on cavitational activity is an important parameter to be evaluated in the search for greater skin permeabilization. A higher cavitational activity implies greater perturbation of the skin,[54,55] and consequently, greater ZnPc penetration.

Surfactants, as SLS, commonly used as LFU coupling medium for skin permeabilization[6,36,56] are known to decrease the number and diameter of gas bubbles formed in the coupling medium.[1,36] This decrease is explained by the ability of surfactants to reduce the surface tension of solutions.[1] The reduced surface tension significantly impacts the oscillation of the cavitation bubbles, stabilizing them, along with the formation of smaller and less energetic population.[57] As a result, the inertial cavitation activity decreases.[1,57] Although DSPE-PEG may have some surfactant properties, DSPE-PEG micelles increased cavitational activity in comparison to the aqueous medium without surfactant (Figure 3).

The increase in cavitational activity caused by the micelles in relation to the water may be related to the reorganization of the micelles as microbubbles during the cavitation. In fact, after irradiation of the micelles with the LFU, a dispersion with multiple populations of particles was observed by DLS, some in the micrometric range (Supplementary material, Figure S4.2). When the micelles encapsulated the ZnPc, the polydispersity of the system was so high that the equipment was unable to complete the analysis. This result suggests that the reorganization of the micelles during the application of the LFU may have expelled some ZnPc molecules to the external environment and forced a new reorganization of the DSPE-PEG and ZnPc molecules or even some precipitation of ZnPc crystals. These modifications resulted in increased cavitation activity compared to the blank micelles, as can be seen from the larger aluminum foil pits area when the ZnPc-loaded micelles were LFU irradiated (Figure 4 and Supplementary material, Figure S4.3). The ZnPc expelled from the micelles could preferentially have reacted with the LFU-generated hydroxyl radicals (from water pyrolysis) and interfered with $KI_3$ absorbance measurements after LFU irradiation.

The cavitational activity generated by the LFU irradiation of the hydrogel was also evaluated because the hydrogel was used as a coupling medium in the LFU skin pretreatment studies. It can be seen in Figure 3 that it was higher than that generated when the micelles were used. The augment of cavitation in the hydrogel coupling medium supports the literature findings, in which the use of hydrogel resulted in a larger area of LTRs, more homogeneously distributed on the skin surface in comparison to the conventional SLS coupling medium.[37] The greater cavitation activity verified in the hydrogel can be explained by the higher energy of the acoustic microbubbles and the lower rate of their dissolution in the more viscous medium. Both factors may cause acoustic microbubbles, formed during an acoustic cycle, to be present in the subsequent cycles, hence increasing their population and the LFU action on the skin.[37] Another explanation is concerning the presence of air trapped in the coupling medium, which can lower the cavitation threshold and act as nuclei for acoustic microbubble growth.[58,59]

The high cavitational activity generated by the hydrogel LFU irradiation and the formation of a large area of LTRs did not result, however, in a greater increase in skin penetration of ZnPc. It can be seen in Table 5 that the pretreatment with the LFU-hydrogel was the one that put the lowest total amount of ZnPc in the skin. Even the passive treatment, only with the micelles, allowed the penetration of a greater amount of ZnPc, despite being restricted to the outer layers of the skin (Figure 5A). It, therefore, appears that the hydrogel that enters the skin with the application of the LFU alters the microenvironment of the LTRs and destabilizes the ZnPc-loaded micelles placed in contact with the skin after the pretreatment, decreasing the amount of solubilized and available ZnPc for penetration. The drug that can penetrate, however, is homogeneously distributed in the epidermis (Figure 5B). This distribution pattern is probably due to the homogeneous distribution of LTRs created on the skin when the hydrogel is used as a coupling medium.[37]

The application of LFU, regardless of the application mode, resulted in a greater penetration of ZnPc in the dermis (Table 5). As non-melanoma and melanoma tumors are originally sited in the epidermis layer;[60,61] higher penetration of ZnPc up to the basal layer of the epidermis is the minimum requirement to secure drug uptake by the target cells and increase sonodynamic activation of the drug for the treatment of skin cancer. Therefore, for in vitro penetration studies, the greater amount of drug accumulated in deeper layers of the skin (ie in the dermis), the better evidence that the drug was capable of spreading throughout the viable epidermis and reaching tumor cells at high concentrations. Note that the drug was not evaluated in the receptor solution of our experiments because ZnPc aggregates in an aqueous medium, which suppresses its fluorescence, preventing its quantification by the analytical method developed.

The ZnPc-loaded micelles, however, allowed a greater amount of ZnPc to penetrate the epidermis passively than the LFU pretreatment, but the drug was trapped in this layer and could not diffuse/partition to the dermis in 6 h of experiment. Due to the high lipophilicity of ZnPc, drug

has probably penetrated through the tortuous routes of intercellular lipids in the stratum corneum, taking longer to reach the balance of distribution and penetration through the skin[62] than when the skin is modified by the application of LFU. Furthermore, it can also be suggested that the high amount of drug quantified in the viable epidermis in the passive experiment for 6 h can be a result of a heterogeneous accumulation of micelle components in the lacunar regions of the stratum corneum, thereby sustaining drug diffusion and partition to the following skin strata and compartments.[63]

Indeed, Figure 5A shows a very heterogeneous distribution of ZnPc after ZnPc-loaded micelles passive administration, concentrated in some furrows of the skin. This result corroborates with others that show that polymeric micelles preferentially accumulate in lacunar regions and appendages of skin.[63,64] The high amount of ZnPc quantified after passive penetration into the epidermis is, therefore, due to the heterogeneous accumulation of the drug on the edge between the stratum corneum and the viable epidermis.

On the other hand, similar amounts of ZnPc in the epidermis and dermis are observed in LFU treatments (Table 5), with a more ZnPc homogeneous distribution throughout the skin than the passive experiment (Figure 5). This suggests that LFU-induced skin permeabilization allowed ZnPc to penetrate the skin by different routes than those used in the absence of LFU and, thus, the drug reached steady state more quickly.

Nonetheless, LFU-ZnPc simultaneous treatment of the skin was the application mode that resulted in the highest amounts of ZnPc in all skin layers (Table 5 and Figure 5). Among the studies that compared simultaneous LFU-sonophoresis to pretreatment or passive treatments, simultaneous sonophoresis also showed to be more advantageous as seen in the present work even though hydrophilic substances were evaluated in those studies.[65,66] This greater penetration observed with the simultaneous protocol is probably due to both drug penetration through LTRs and LFU-induced convective forces and acoustic streaming.[1,2,67]

It is possible to estimate the contribution of convection and acoustic transmission in ZnPc penetration by LFU-ZnPc simultaneous treatment taking into considering that (i) in the LFU pretreatment protocol, the penetration of the drug occurs under the domain of LTRs only; and (ii) in the simultaneous application experiments, ZnPc penetration relies on both LTRs formation and LFU-induced convective and acoustic streaming processes. Therefore, the difference between ZnPc flux after simultaneous treatment ($110\ ng.cm^{-2}.h^{-1}$) and that flux after pretreatment ($30\ ng.cm^{-2}.h^{-1}$) results in the contribution of the convective and acoustic flow to the penetration of ZnPc. Thus, it was estimated that the LFU convective and acoustic flow contributed to about 70% of ZnPc skin penetration in simultaneous LFU treatment.

It is important to underline that drug penetration via LTRs was estimated as a function of the sonophoresis pretreatment experiments performed with a hydrogel as a coupling media. Thereby, the influence of micelles and DSPE-PEG molecules in the contribution of LTRs to ZnPc skin penetration was not taken into account, but they were used as the coupling medium in the LFU-ZnPc simultaneous experiment. DSPE-PEG molecules have shown the ability to modify skin barrier properties, fuse, and diffuse across the stratum corneum, disrupting the lipid packaging of the skin lipid matrix and promoting a change in skin solubility properties relative to the permeant drug.[68] Simultaneous treatment with ZnPc-loaded micelles pushes these structures into the skin, and may, therefore, alter the characteristics and permeability of LTRs and non-LTRs and affect ZnPc partition and diffusion through the skin, compared to LFU-hydrogel pretreatment.

Having known the influence of LFU type of application on ZnPc-loaded micelles skin penetration, LFU associated with these micelles was then investigated as an energy source for the production of ROS in SDT. Therefore, oxygen singlet formation, a highly cytotoxic agent responsible for inducing irreversible damage in cancerous cells and tissues,[69,70] was evaluated. LFU irradiation of ZnPc-loaded micelles significantly increased singlet oxygen generation compared to LFU irradiation of a buffer solution, as can be seen in Figure 6. It is believed that the acoustic energy and sonoluminescence derived from ultrasonic cavitation is responsible for the excitation of the ZnPc, resulting in the formation of singlet oxygen when the energy is released on its return to the ground state.[71] The irradiation of Rose Bengal microbubbles,[72] indocyanine green microbubbles[73] and metalloporphyrins nanoparticles[16] for at least 30 s with 1 MHz ultrasound, also resulted in the production of singlet oxygen. The generation of singlet oxygen resulting from irradiation with LFU has only been described recently, by the irradiation of MnWOx bimetallic oxide nanoparticles with a 40 kHz ultrasound.[7] It is the first time that the formation of singlet oxygen is observed after irradiation of an organic sensitizer using LFU of 20 kHz.

The generation of singlet oxygen derived from the irradiation of blank micelles, which did not contain the

sonosensitizing agent (Figure 6), is, however, intriguing. We hypothesize that the DSPE-PEG micelle, which composition is very similar to that of microbubbles reported in the literature,[74,75] could trap gas in its hydrophobic nucleus when subjected to LFU sonication, hence assisting sonoluminescence and $^1O_2$ production.[71] There is no consensus on the precise mechanisms of generation of ROS assisted by cavitation microbubbles[71] although the production of singlet oxygen has been reported when some nanostructured systems such as microbubbles[71] and inorganic nanoparticles[76] were irradiated with 1 MHz ultrasound for at least 2 min. Therefore, further investigation is needed to evaluate the potential of blank DSPE-PEG micelles herein developed as nanobubbles for SDT.

As ROS in SDT is expected to cause a wide range of tumor tissue damages and cancer cell death, skin lipid peroxidation assay and preliminary in vitro cell viability tests were carried out to demonstrate the feasibility of LFU as an energy source for sonodynamic production of ROS.

Three-fold enhanced lipid peroxidation was observed in the skin tissue pre-treated with LFU-ZnPc simultaneous sonophoresis (Figure 7). This result indicates that in the presence of the sensitizing drug a sonodynamic response could be mediated by LFU. As the LFU-ZnPc simultaneous treatment resulted in higher penetration (Table 5) and better distribution (Figure 5D) of the ZnPc in the skin, enhanced lipid peroxidation could be verified because of the improved bioavailability of the sensitizing drug in the skin tissue.

Once ZnPc is within the skin after penetration, it is believed that not only $^1O_2$ can be generated in the LFU presence, but also long-time free radicals derived from the sonosensitizing molecule could be formed by hemolytic cleavage or reactions of it with as-formed hydrogen atoms and/or hydroxyl radicals and other solutes there present.[69] Further studies to evaluate the potential of ZnPc to be converted into radical species in the presence of LFU are needed, or even in search of new sonosensitizers, more susceptible to sonodynamic activity.

Cell viability results (Figure 8) showed that LFU induced the death of about 40% of melanoma cells when associated with ZnPc-loaded micelles. It is worthy to emphasize that the experimental setup used for this study did not provide the complete delivery of the ultrasound energy to the monolayered cells because of the (i) longer wavelength of LFU (in comparison to high-frequency ultrasound)[1], (ii) transducer-to-microplate distance; and (iii) large volume of coupling medium necessary for both the well-functioning of the LFU and the avoidance of thermal effects. The dispersion of the LFU waves and energy due to these factors could have led to reduced cavitation process close to the monolayer cells, hence diminishing the sonodynamic effects onto the cells. Any reduction in the percentage of viable cells was observed in the blank micelles group control despite the production of $^1O_2$ detected using two specific chemical methods for this purpose (Figure 6A and 6B). Probably the poor delivery of the LFU energy from the experimental configuration could have led to a reduction in $^1O_2$ production in the blank micelle control group. Nevertheless, the experimental configuration for the LFU application designed was able to show LFU-induced SDT effects in association with ZnPc-loaded micelles on melanoma cells. Further studies have been conducted to find an optimal experimental setup for better evaluation of the LFU-mediated SDT in cell culture. Also, the identification of other ROS and radical species derived from the sensitizing drug is necessary to further demonstrate LFU potential in topical SDT aiming for the treatment of skin tumors.

## Conclusion

Nanometric-sized, monodisperse DSPE-PEG micelles developed allowed the solubilization and topical administration of lipophilic ZnPc. The use of ZnPc-loaded micelles as a coupling medium for the application of LFU, designated in this work as LFU-ZnPc simultaneous treatment, provided greater penetration and better distribution of ZnPc in the deeper layers of the skin when compared to passive or LFU pretreatment. The micellar system was able to improve cavitation activity and elicit the formation of singlet oxygen under LFU irradiation. Moreover, the application of LFU in the skin previously treated with LFU-ZnPc showed to cause lipid peroxidation of the skin tissue and induced cell death in association with ZnPc-loaded micelles. Therefore, the application of LFU on the skin has the double potential of permeabilizing it and providing the treatment of skin tumors by SDT.

## Abbreviations

LFU, low-frequency ultrasound; SDT, sonodynamic therapy; LTR, localized transport regions.

## Acknowledgments

The author would like to thank the São Paulo Research Foundation – FAPESP (grant number 2014/22451-7 and 2017/17442-7), the National Council for Scientific and Technological Development – CNPq (grant number 421824/2016-6), the National Institute of Science and Technology in Pharmaceutical Nanotechnology – INCT

NANOFARMA (FAPESP grant number 2014/50928-2 and CNPq grant number 465687/2014-8), and the Coordination for the Improvement of Higher Education Personnel – CAPES (grant number 001) for financial support. The authors also thank Patrícia Sper Simão and José Roberto Jabor for the technical support with the lab experiments.

## Disclosure

The authors report no conflicts of interest in this work.

## References

1. Polat BE, Hart D, Langer R, Blankschtein D. Ultrasound-Mediated Transdermal Drug Delivery: mechanisms, Scope, and Emerging Trends. *J Controlled Release*. 2011;152(3):330–348. doi:10.1016/j.jconrel.2011.01.006
2. Mitragotri S, Kost J. Low-Frequency Sonophoresis: A Review. *Adv Drug Delivery Rev*. 2004;56(5):589–601. doi:10.1016/j.addr.2003.10.024
3. Polat BE, Figueroa PL, Blankschtein D, Langer R. Transport Pathways and Enhancement Mechanisms Within Localized and Non-Localized Transport Regions in Skin Treated with Low-Frequency Sonophoresis and Sodium Lauryl Sulfate. *J Pharm Sci*. 2011;100(2):512–529. doi:10.1002/jps.22280
4. Wolloch L, Kost J. The Importance of Microjet vs Shock Wave Formation in Sonophoresis. *J Controlled Release*. 2010;148(2):204–211. doi:10.1016/j.jconrel.2010.07.106
5. Kushner K, Blankschtein D, Langer R. Experimental Demonstration of the Existence of Highly Permeable Localized Transport Regions in Low-Frequency Sonophoresis. *J Pharm Sci*. 2004;93(11):2733–2745. doi:10.1002/jps.20173
6. Polat BE, Deen WM, Langer R, Blankschtein D. A physical mechanism to explain the delivery of chemical penetration enhancers into skin during transdermal sonophoresis — insight into the observed synergism. *J Controlled Release*. 2012;158(2):250–260. doi:10.1016/j.jconrel.2011.11.008
7. Gong F, Cheng L, Yang N, et al. Ultrasmall Oxygen-Deficient Bimetallic Oxide MnWO X Nanoparticles for Depletion of Endogenous GSH and Enhanced Sonodynamic Cancer Therapy.*Adv Mater*. 2019;31(23):1900730. doi:10.1002/adma.201900730
8. Behzadpour N, Ranjbar A, Azarpira N, Sattarahmady N. Development of a Composite of Polypyrrole-Coated Carbon Nanotubes as a Sonosensitizer for Treatment of Melanoma Cancer Under Multi-Step Ultrasound Irradiation. *Ultrasound Med Biol*. 2020;00(00):1–13. doi:10.1016/j.ultrasmedbio.2020.05.003
9. Soratijahromi E, Mohammadi S, Dehdari Vais R, Azarpira N, Sattarahmady N. Photothermal/Sonodynamic Therapy of Melanoma Tumor by a Gold/Manganese Dioxide Nanocomposite: in Vitro and in Vivo Studies. *Photodiagnosis Photodynamic Therapy*. 2020;31(May):101846. doi:10.1016/j.pdpdt.2020.101846
10. Lafond M, Yoshizawa S, Umemura S. Sonodynamic Therapy: advances and Challenges in Clinical Translation. *J Ultrasound Med*. 2019;38(3):567–580. doi:10.1002/jum.14733
11. Aksel M, Bozkurt-Girit O, Bilgin MD. Pheophorbide A-Mediated Sonodynamic, Photodynamic and Sonophotodynamic Therapies against Prostate Cancer. *Photodiagnosis Photodynamic Therapy*. 2020;31(January):101909. doi:10.1016/j.pdpdt.2020.101909
12. Shen Y, Ou J, Chen X, et al. An in Vitro Study on Sonodynamic Treatment of Human Colon Cancer Cells Using Sinoporphyrin Sodium as Sonosensitizer. *BioMed Eng OnLine*. 2020;19(1):52. doi:10.1186/s12938-020-00797-w
13. Wan G-Y, Liu Y, Chen B-W, et al. Recent Advances of Sonodynamic Therapy in Cancer Treatment. *Cancer Biol Med*. 2016;13(3):325–338. doi:10.20892/j.issn.2095-3941.2016.0068
14. Liu Z, Li J, Jiang Y, Wang D. Multifunctional Nanocapsules on a Seesaw Balancing Sonodynamic and Photodynamic Therapies against Superficial Malignant Tumors by Effective Immune-Enhancement. *Biomaterials*. 2019;218(May):119251. doi:10.1016/j.biomaterials.2019.119251
15. McEwan C, Nesbitt H, Nicholas D, et al. Comparing the Efficacy of Photodynamic and Sonodynamic Therapy in Non-Melanoma and Melanoma Skin Cancer. *Bioorganic Med Chem*. 2016;24(13):3023–3028. doi:10.1016/j.bmc.2016.05.015
16. Ma A, Chen H, Cui Y, et al. Metalloporphyrin Complex-Based Nanosonosensitizers for Deep-Tissue Tumor Theranostics by Noninvasive Sonodynamic Therapy. *Small*. 2019;15(5):1804028. doi:10.1002/smll.201804028
17. Wu S-K, Santos MA, Marcus SL. MR-Guided Focused Ultrasound Facilitates Sonodynamic Therapy with 5-Aminolevulinic Acid in a Rat Glioma Model. *Sci Rep*. 2019;9(1):1–10. doi:10.1038/s41598-019-46832-2
18. Liu M, Khan AR, Ji J, Lin G, Zhao X, Zhai ZG. Crosslinked self-assembled nanoparticles for chemo-sonodynamic combination therapy favoring antitumor, antimetastasis management and immune responses.*J Controlled Release*. 2018;290(May):150–164. doi:10.1016/j.jconrel.2018.10.007
19. Obrienjr WD. Ultrasound–Biophysics Mechanisms.*Progress Biophysics Mol Biol*. 2007;93(1–3):212–255. doi:10.1016/j.pbiomolbio.2006.07.010
20. Daffertshofer M, Gass A, Ringleb P, et al. Transcranial Low-Frequency Ultrasound-Mediated Thrombolysis in Brain Ischemia: increased Risk of Hemorrhage with Combined Ultrasound and Tissue Plasminogen Activator - Results of a Phase II Clinical Trial. *Stroke*. 2005;36(7):1441–1446. doi:10.1161/01.STR.0000170707.86793.1a
21. Ahmadi F, McLoughlin IV, Chauhan S, ter-Haar G. Bio-Effects and Safety of Low-Intensity, Low-Frequency Ultrasonic Exposure. *Progress Biophysics Mol Biol*. 2012;108(3):119–138. doi:10.1016/j.pbiomolbio.2012.01.004
22. Xu H, Sun X, Yao J, et al. The Decomposition of Protoporphyrin IX by Ultrasound Is Dependent on the Generation of Hydroxyl Radicals. *Ultrasonics Sonochemistry*. 2015;27:623–630. doi:10.1016/j.ultsonch.2015.04.024
23. Garcia AM, Alarcon E, Muñoz M, Scaiano JC, Edwards AM, Lissi LE. Photophysical behaviour and photodynamic activity of zinc phthalocyanines associated to liposomes. *Photochem Photobiol Sci*. 2011;10(4):507–514. doi:10.1039/c0pp00289e
24. Md S, Haque S, Madheswaran T, et al. Lipid Based Nanocarriers System for Topical Delivery of Photosensitizers. *Drug Discovery Today*. 2017;22(8):1274–1283. doi:10.1016/j.drudis.2017.04.010
25. Dalmolin L, Lopez R. Nanoemulsion as a Platform for Iontophoretic Delivery of Lipophilic Drugs in Skin Tumors. *Pharmaceutics*. 2018;10(4):214. doi:10.3390/pharmaceutics10040214
26. de Lima R, Tedesco AC, da Silva RS, Lawrence MJ. Ultradeformable liposome loaded with zinc phthalocyanine and [Ru(NH.NHq)(tpy)NO] 3+ for photodynamic therapy by topical application. *Photodiagnosis Photodynamic Therapy*. 2017;19:184–193. doi:10.1016/j.pdpdt.2017.05.013
27. Che J, Okeke C, Hu Z-B, Xu J. DSPE-PEG: A Distinctive Component in Drug Delivery System.*Current Pharm Design*. 2015;21(12):1598–1605. doi:10.2174/1381612821666150115144003
28. Yotsumoto K, Ishii K, Kokubo M, Yasuoka S. Improvement of the Skin Penetration of Hydrophobic Drugs by Polymeric Micelles. *Int J Pharm*. 2018;553(1–2):132–140. doi:10.1016/j.ijpharm.2018.10.039
29. Bachhav YG, Mondon K, Kalia YN, Gurny R, Möller MM. Novel micelle formulations to increase cutaneous bioavailability of azole antifungals.*J Controlled Release*. 2011;153(2):126–132. doi:10.1016/j.jconrel.2011.03.003

30. Loan Honeywell-Nguyen P, de Graaff AM, Wouter Groenink H, Bouwstra JA. The in Vivo and in Vitro Interactions of Elastic and Rigid Vesicles with Human Skin. *Biochimica Et Biophysica Acta*. 2002;1573(2):130–140. doi:10.1016/S0304-4165(02)00415-4
31. Sirsi SR, Borden MA. State-of-the-Art Materials for Ultrasound-Triggered Drug Delivery. *Adv Drug Delivery Rev*. 2014;72:3–14. doi:10.1016/j.addr.2013.12.010
32. Sezgin Z, Yuksel N, Baykara BT. Preparation and characterization of polymeric micelles for solubilization of poorly soluble anticancer drugs.*Eur J Pharm Biopharm*. 2006;64(3):261–268. doi:10.1016/j.ejpb.2006.06.003
33. Arora D, Nanda S. Quality by Design Driven Development of Resveratrol Loaded Ethosomal Hydrogel for Improved Dermatological Benefits via Enhanced Skin Permeation and Retention. *Int J Pharm*. 2019;567(May):118448. doi:10.1016/j.ijpharm.2019.118448
34. Ebrahiminia A, Mokhtari-Dizaji M, Toliyat T. Dual Frequency Cavitation Event Sensor with Iodide Dosimeter. *Ultrasonics Sonochemistry*. 2016;28:276–282. doi:10.1016/j.ultsonch.2015.07.005
35. Xu Z, Ma CY, Xu JY, Liu XJ. Ultrasonics Sonochemistry Dynamical Properties of Iodine Release in Potassium Iodide Solution under Combination of Ultrasound and Light Irradiations. *Sci Rep*. 2009;16:475–480. doi:10.1016/j.ultsonch.2008.12.008
36. Mitragotri S, Ray D, Farrell J, et al. Synergistic Effect of Low-Frequency Ultrasound and Sodium Lauryl Sulfate on Transdermal Transport.*J Pharm Sci*. 2000;89(7):892–900. doi:10.1002/1520-6017(200007)89:7<892::AID-JPS6>3.0.CO;2-V
37. Pereira TA, Ramos DN, Lopez RFV. Hydrogel Increases Localized Transport Regions and Skin Permeability during Low Frequency Ultrasound Treatment. *Sci Rep*. 2017;7(1):1–10. doi:10.1038/srep44236
38. Liang L, Xie S, Jiang L, Jin H, Li S, Liu J. The Combined Effects of Hematoporphyrin Monomethyl Ether-SDT and Doxorubicin on the Proliferation of QBC939 Cell Lines. *Ultrasound Med Biol*. 2013;39(1):146–160. doi:10.1016/j.ultrasmedbio.2012.08.017
39. Yumita N, Iwase Y, Watanabe T, et al. Involvement of Reactive Oxygen Species in the Enhancement of Membrane Lipid Peroxidation by Sonodynamic Therapy with Functionalized Fullerenes. *Anticancer Res*. 2014;34(11):6481–6487.
40. Uzarski JS, DiVito MD, Wertheim JA, Miller WM. Essential Design Considerations for the Resazurin Reduction Assay to Noninvasively Quantify Cell Expansion within Perfused Extracellular Matrix Scaffolds. *Biomaterials*. 2017;129(June):163–175. doi:10.1016/j.biomaterials.2017.02.015
41. Lukyanov AN, Gao Z, Mazzola L, Torchilin VP. Polyethylene Glycol-Diacyllipid Micelles Demonstrate Increased Acculumation in Subcutaneous Tumors in Mice. *Pharmaceutical Res*. 2002;19(10):1424–1429. doi:10.1023/A:1020488012264
42. Sezgin-bayindir Z, Ergin AD, Parmaksiz M, Elcin AE, Elcin YM, Yuksel N. Evaluation of various block copolymers for micelle formation and brain drug delivery: in vitro characterization and cellular uptake studies. *J Drug Delivery Sci Tech*. 2016;36:120–129. doi:10.1016/j.jddst.2016.10.003
43. Sun F, Jaspers TCC, van Hasselt PM, Hennink WE, van Nostrum CF. A Mixed Micelle Formulation for Oral Delivery of Vitamin K. *Pharmaceutical Res*. 2016;33(9):2168–2179. doi:10.1007/s11095-016-1954-9
44. Elsaid Z, Taylor KMG, Puri S, et al. Mixed Micelles of Lipoic Acid-Chitosan-Poly(Ethylene Glycol) and Distearoylphosphatidylethanolamine-Poly(Ethylene Glycol) for Tumor Delivery. *Eur J Pharm Sci*. 2017;101:228–242. doi:10.1016/j.ejps.2017.02.001
45. Gill KK, Kaddoumi A, Nazzal S. PEG–Lipid Micelles as Drug Carriers: physiochemical Attributes, Formulation Principles and Biological Implication. *J Drug Targeting*. 2015;23(3):222–231. doi:10.3109/1061186X.2014.997735
46. Lukyanov AN, Torchilin VP. Micelles from Lipid Derivatives of Water-Soluble Polymers as Delivery Systems for Poorly Soluble Drugs. *Adv Drug Delivery Rev*. 2004;56(9):1273–1289. doi:10.1016/j.addr.2003.12.004
47. Hsu H, Han Y, Cheong M, Král P, Hong S. Dendritic PEG Outer Shells Enhance Serum Stability of Polymeric Micelles. *Nanomedicine*. 2018;14(6):1879–1889. doi:10.1016/j.nano.2018.05.010
48. Johnsson M, Hansson P, Edwards EK. Spherical Micelles and Other Self-Assembled Structures in Dilute Aqueous Mixtures of Poly(Ethylene Glycol) Lipids.*J Physical Chem B*. 2001;105(35):8420–8430. doi:10.1021/jp011088l
49. Sibata MN, Tedesco AC, Marchetti JM. Photophysicals and Photochemicals Studies of Zinc(II) Phthalocyanine in Long Time Circulation Micelles for Photodynamic Therapy Use. *Eur J Pharm Sci*. 2004;23(2):131–138. doi:10.1016/j.ejps.2004.06.004
50. Lundquist A, Wessman P, Rennie AR, Edwards EK. Melittin–Lipid interaction: A comparative study using liposomes, micelles and bilayerdisks.*Biochimica Et Biophysica Acta (BBA) - Biomembranes*. 2008;1778(10):2210–2216. doi:10.1016/j.bbamem.2008.05.009
51. Johnsson M, Edwards EK. Liposomes, Disks, and Spherical Micelles: aggregate Structure in Mixtures of Gel Phase Phosphatidylcholines and Poly(Ethylene Glycol)-Phospholipids.*Biophysical J*. 2003;85(6):3839–3847. doi:10.1016/S0006-3495(03)74798-5
52. de Oliveira de Siqueira LB, da Silva Cardoso V, Rodrigues IA. Development and evaluation of zinc phthalocyanine nanoemulsions for use in photodynamic therapy for Leishmania spp.. *Nanotechnology*. 2017;28(6):065101. doi:10.1088/1361-6528/28/6/065101
53. Dahlan A, Alpar HO, Murdan S. An Investigation into the Combination of Low Frequency Ultrasound and Liposomes on Skin Permeability. *Int J Pharmaceutics*. 2009;379(1):139–142. doi:10.1016/j.ijpharm.2009.06.011
54. Tang H, Wang CCJ, Blankschtein D, Langer R. An Investigation of the Role of Cavitation in Low-Frequency Ultrasound-Mediated Transdermal Drug Transport.*Pharmaceutical Res*. 2002;19(8):1160–1169. doi:10.1023/A:1019898109793
55. Tezel A, Sens A, Mitragotri S. Investigations of the role of cavitation in low-frequency sonophoresis using acoustic spectroscopy.*J Pharm Sci*. 2002;91(2):444–453. doi:10.1002/jps.10024
56. Seto JE, Polat BE, Lopez RFV, Blankschtein D, Langer R. Effects of Ultrasound and Sodium Lauryl Sulfate on the Transdermal Delivery of Hydrophilic Permeants: comparative in Vitro Studies with Full-Thickness and Split-Thickness Pig and Human Skin. *J Controlled Release*. 2010;145(1):26–32. doi:10.1016/j.jconrel.2010.03.013
57. Lee J, Kentish S, Matula TJ, Ashokkumar M. Effect of Surfactants on Inertial Cavitation Activity in a Pulsed Acoustic Field. *J Phys Chem B*. 2005;109(35):16860–16865. doi:10.1021/jp0533271
58. Tamarov K, Sviridov A, Xu W, et al. Nano Air Seeds Trapped in Mesoporous Janus Nanoparticles Facilitate Cavitation and Enhance Ultrasound Imaging. *ACS Applied Mater Interfaces*. 2017;9(40):35234–35243. doi:10.1021/acsami.7b11007
59. Peng Y, Li Q, Seekell RR, Kheir JN, Porter TM, Polizzotti BD. Tunable Nonlinear Acoustic Reporters Using Micro- and Nanosized Air Bubbles with Porous Polymeric Hard Shells. *ACS Applied Materials & Interfaces*. 2019;11(1):7–12. doi:10.1021/acsami.8b16737
60. Chummun S, McLean NR. The Management of Malignant Skin Cancers. *Surg (United Kingdom)*. 2017;35(9):519–524. doi:10.1016/j.mpsur.2017.06.013
61. Craythorne E, Al-Niami F. Skin Cancer. *Med (United Kingdom)*. 2017;45(7):431–434. doi:10.1016/j.mpmed.2017.04.003
62. Mitragotri S, Blankschtein D, Langer R. Transdermal Drug Delivery Using Low-Frequency Sonophoresis. *Pharmaceutical Res*. 1996;13(3):411–420. doi:10.1023/A:1016096626810

63. Maibach HI, Dragicevic N. Percutaneous Penetration Enhancers Chemical Methods in Penetration Enhancement. In: Dragicevic N, Maibach HI, editors.*Springer-Verlag Berlin Heidelberg*. New York;2016.
64. Dragicevic N, Maibach H. Combined Use of Nanocarriers and Physical Methods for Percutaneous Penetration Enhancement. *Adv Drug Delivery Rev*. 2018;127:58–84. doi:10.1016/j.addr.2018.02.003
65. Tezel A, Dokka S, Kelly S, Hardee GE, Mitragotri S. Topical Delivery of Anti-Sense Oligonucleotides Using Low-Frequency Sonophoresis. *Pharm Res*. 2004;21(12):2219–2225. doi:10.1007/s11095-004-7674-6
66. Manikkath J, Hegde AR, Kalthur G, Parekh HS, Mutalik S. Influence of Peptide Dendrimers and Sonophoresis on the Transdermal Delivery of Ketoprofen. *Int J Pharm Sci Res*. 2017;521(2):110–119. doi:dx.doi.10.1016/j.ipharm.2017.02.002
67. Ita IK. Recent progress in transdermal sonophoresis.*Pharm Dev Tech*. 2017;22(4):458–466. doi:10.3109/10837450.2015.1116566
68. Mahmoud NN, Alhusban AA, Ali JI, Al-Bakri AG, Hamed R, Khalil EA. Preferential Accumulation of Phospholipid-PEG and Cholesterol-PEG Decorated Gold Nanorods into Human Skin Layers and Their Photothermal-Based Antibacterial Activity. *Sci Rep*. 2019;9(1):5796. doi:10.1038/s41598-019-42047-7
69. Rosenthal I, Sostaric JZ, Sonodynamic Therapy: RP. A Review of the Synergistic Effects of Drugs and Ultrasound. *Ultrason Sonochem*. 2004;11(6):349–363. doi:10.1016/j.ultsonch.2004.03.004
70. Costley D, Mc Ewan C, Fowley C, et al. Treating Cancer with Sonodynamic Therapy: A Review. *Int J Hyperthermia*. 2015;31(2):107–117. doi:10.3109/02656736.2014.992484
71. Beguin E, Shrivastava S, Dezhkunov NV, McHale AP, Callan JF, Stride E. Direct Evidence of Multibubble Sonoluminescence Using Therapeutic Ultrasound and Microbubbles. *ACS Applied Materi Interfaces*. 2019;11(22):19913–19919. doi:10.1021/acsami.9b07084
72. McEwan C, Owen J, Stride E, et al. Oxygen Carrying Microbubbles for Enhanced Sonodynamic Therapy of Hypoxic Tumours. *J Controlled Release*. 2015;203:51–56. doi:10.1016/j.jconrel.2015.02.004
73. Ma R, Wu Q, Si T, Chang S, Xu RX. Oxygen and Indocyanine Green Loaded Microparticles for Dual-Mode Imaging and Sonodynamic Treatment of Cancer Cells. *Ultrasonics Sonochemistry*. 2017;39:197–207. doi:10.1016/j.ultsonch.2017.03.019
74. Lozano MM, Longo ML. Microbubbles Coated with Disaturated Lipids and DSPE-PEG2000: phase Behavior, Collapse Transitions, and Permeability. *Langmuir*. 2009;25(6):3705–3712. doi:10.1021/la803774q
75. Owen J, Kamila S, Shrivastava S. The Role of PEG-40-Stearate in the Production, Morphology, and Stability of Microbubbles. *Langmuir*. 2019;35(31):10014–10024. doi:10.1021/acs.langmuir.8b02516
76. Harada A, Ono M, Yuba E, Kono K. Titanium Dioxide Nanoparticle-Entrapped Polyion Complex Micelles Generate Singlet Oxygen in the Cells by Ultrasound Irradiation for Sonodynamic Therapy. *Biomater Sci*. 2013;1(1):65–73. doi:10.1039/C2BM00066K

**International Journal of Nanomedicine** Dovepress

## Publish your work in this journal

The International Journal of Nanomedicine is an international, peer-reviewed journal focusing on the application of nanotechnology in diagnostics, therapeutics, and drug delivery systems throughout the biomedical field. This journal is indexed on PubMed Central, MedLine, CAS, SciSearch®, Current Contents®/Clinical Medicine, Journal Citation Reports/Science Edition, EMBase, Scopus and the Elsevier Bibliographic databases. The manuscript management system is completely online and includes a very quick and fair peer-review system, which is all easy to use. Visit http://www.dovepress.com/testimonials.php to read real quotes from published authors.

**Submit your manuscript here:** https://www.dovepress.com/international-journal-of-nanomedicine-journal